Contents lists available at ScienceDirect

Nano Today

Nano-enabled DNA supramolecular sealant for soft tissue surgical applications

Manshan Xie [a], Yunhua Chen [a,b,c,d,*], Qian Yang [a], Qingtao Li [e], Runlin Zhang [a,b], Wenzhi Bi [a], Yong-Guang Jia [a,b], Paul K. Chu [f], Huaiyu Wang [g,**], Xuetao Shi [a,b,c,d,*]

[a] National Engineering Research Center for Tissue Restoration and Reconstruction, South China University of Technology, Guangzhou 510006, China
[b] School of Materials Science and Engineering, South China University of Technology, Guangzhou 510641, China
[c] Key Laboratory of Biomedical Materials and Engineering of the Ministry of Education, South China University of Technology, Guangzhou 510006, China
[d] Key Laboratory of Biomedical Engineering of Guangdong Province, and Innovation Center for Tissue Restoration and Reconstruction, South China University of Technology, Guangzhou 510006, China
[e] School of Medicine, South China University of Technology, Guangzhou 510006, China
[f] Department of Physics, Department of Materials Science and Engineering, and Department of Biomedical Engineering, City University of Hong Kong, Tat Chee Avenue, Kowloon, Hong Kong Special Administrative Region
[g] Center for Human Tissues and Organs Degeneration, Shenzhen Institutes of Advanced Technology, Chinese Academy of Sciences, Shenzhen 518055, China

ARTICLE INFO

ABSTRACT

Bioadhesives or sealants have received considerable attention for suture-less wound sealing. However, most adhesive biomaterials involve complex molecular designs which lack dynamic mechanical properties, inherent hemostasis, as well as the capability of preventing postsurgical tissue adhesion. Herein, a nano-enabled supramolecular hydrogel sealant based on complementary DNA duplexes combined with multiple physicochemical crosslinks is designed and demonstrated. This supramolecular sealant exhibits excellent dynamic reversibility, low swelling, and wet adhesive properties. It can achieve rapid sealing of damaged tissues, blood coagulation, as well as hemostasis. Furthermore, DNA molecules endow the sealant with promising capabilities of preventing protein absorption, cell adhesion and postsurgical tissue adhesion. The in vivo evaluation based on the gastric perforation repair model shows that the sealant can improve granulation tissue growth, collagen deposition, and vascularization and facilitate gastric perforation closure. The nano-enabled DNA supramolecular hydrogel sealant represents a promising alternative for gastric perforation repair and has large clinical potential pertaining to suture-less repair of soft tissues.

Data availability: The data reported in this manuscript are available upon request.

Introduction

Injury of soft tissues caused by surgery and accidental trauma are often accompanied by uncontrollable bleeding [1] and timely wound closure and hemostasis are crucial. Traditional wound repair methods using sutures, surgical staples, and clips are widely used but these mechanical techniques may fail to close wounds completely leading to extravasation of tissue fluids and may also cause secondary damage to the surrounding tissues [2,3]. In light of these shortcomings of traditional wound treatment methods, sutureless bioadhesives such as cyanoacrylate-based adhesives [4], fibrin sealants [5,6], albumin-based bioglue [7], and poly(ethylene glycol) (PEG)-based DuraSeal [8] or Coseal [9] have attracted attention. They can physically adhere to tissues and seal the wounds without damaging surrounding tissues. For example, cyanoacrylate-based sealants are easy to use and adhere quickly and strongly to tissues by providing a physical barrier to prevent exudation of blood and body fluids, thus preventing wounds from infection by bacteria in the external environment. However, the significant cytotoxicity and intrinsic brittle characteristics limit the application of these types of adhesives in visceral wounds [10].

PEG-based adhesives with the hydroxysuccinimide/thiol chemistry can seal wounds seamlessly, avoid additional post-operative damage, and even prevent postoperative adhesion [11,12]. However, owing to the high degree of hydrophilicity, they can cause

* Corresponding authors at: National Engineering Research Center for Tissue Restoration and Reconstruction, South China University of Technology, Guangzhou 510006, China.
** Corresponding author.
E-mail addresses: msyhchen@scut.edu.cn (Y. Chen), hy.wang1@siat.ac.cn (H. Wang), shxt@scut.edu.cn (X. Shi).
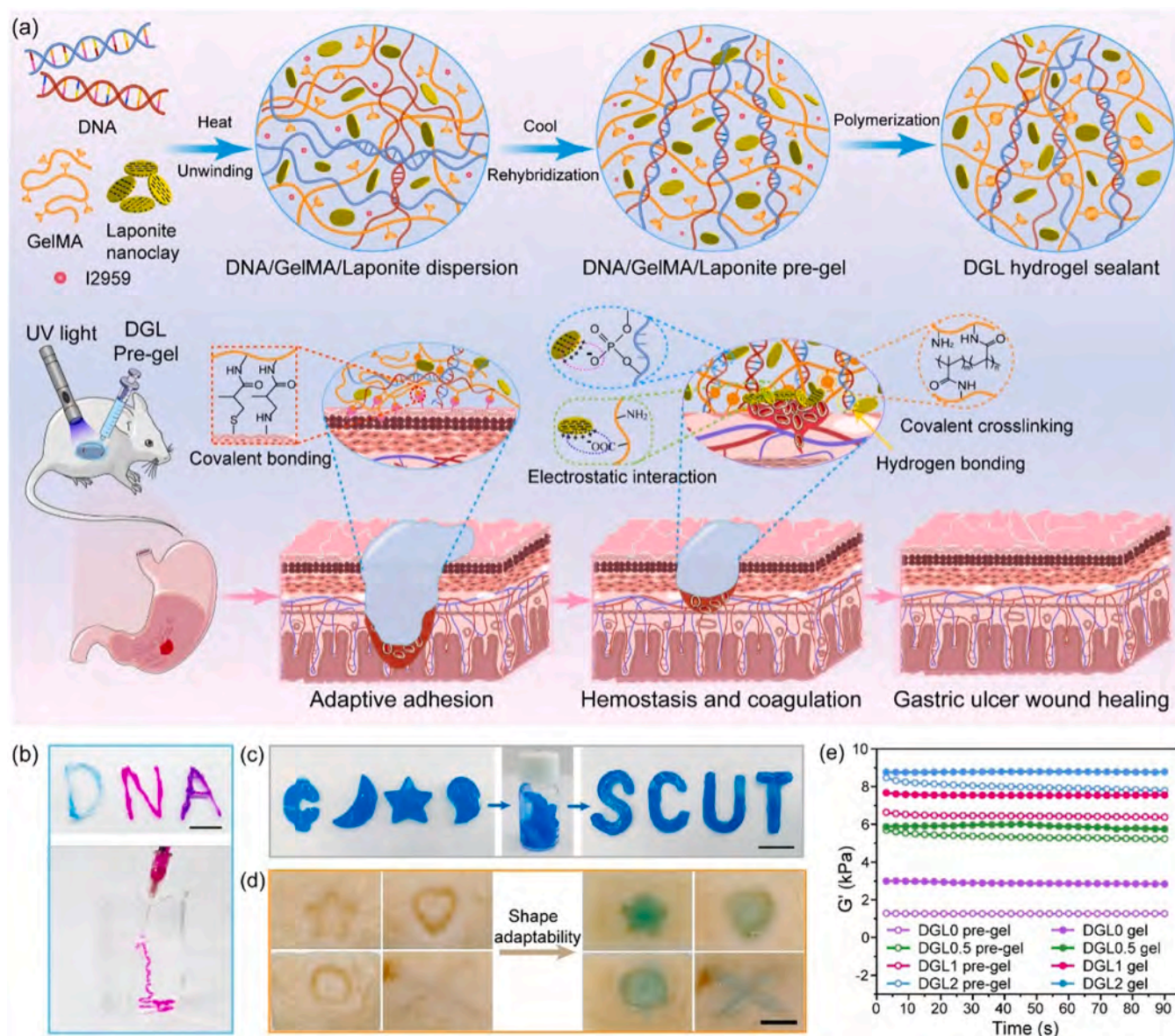
Fig. 1. Design of the DGL sealant for surgical applications: (a) Schematic showing the preparation of DGL sealant and gastric perforation wound healing. (b) Injectability of DGL pre-gel (rhodamine-B and methylene blue staining). (c) DGL pre-gel prepared with different shape by molding and being re-shapeable. (d) DGL pre-gel adapting to the scratch shape on pigskin. Scale bar: 1 cm. (e) Storage moduli of the DGL pregels before and after polymerization.

mechanical failure and induce tissue compression after the water swelling, leading to severe inflammatory response in some cases [13]. In contrast, fibrin glues composed of fibrinogens and thrombin have good degradation properties, but lack good dynamic mechanical properties and complicated processes are required to get rid of pathogens such as viruses and prions [14]. Moreover, most bioadhesives cannot undergo mechanical recovery after the static cross-linked networks are damaged in the dynamic wound environment, which will lead to wound closure failure. Dynamic bioadhesives based on supramolecular crosslinking mechanisms have shown great potential [15]. A general approach is to graft supramolecular moieties onto polymer chains and construction of reversible cross-linked networks based on self-assembly of polymers is triggered under the stimulation of temperature, light, or small molecules [16,17]. For example, a supramolecular hydrogel dressing composed of poly(*N*-isopropylacrylamide)-adenine and quaternized chitosan-graft-β-cyclodextrin *via* host-guest interactions and hydrogen bonds has been developed [18]. This thermoresponsive adhesive hydrogel exhibits excellent self-healing, antibacterial, and hemostatic abilities

while promoting wound contraction and closure. However, most supramolecular bioadhesives still have drawbacks such as weak wet adhesion and complex synthesis.

DNA macromolecules featuring precise base-pair recognition are regarded as easy building blocks to construct dynamic hydrogel materials and the ultrahigh molecular weight of DNA facilitates formation of strong supramolecular networks with an energy dissipation mechanism [19,20]. Notably, DNA crosslinking hydrogels are relatively strong compared to most supramolecular hydrogels. They also have promising thixotropic properties and can be easily molded into the desired shape by injection [21–23]. The high permeability of DNA hydrogels allows fast nutrient transport for cell growth and provides the possibility to develop interpenetrating double network matrices [24,25]. Moreover, the hydrophilic DNA chains bear abundant anionic monophosphates [26–28], which may be utilized to prevent postsurgical tissue adhesion. Considering these unique characteristics, it is highly interesting and desirable to design a DNA-based sealant that boasts strong tissue adhesion, injectable and self-healing properties, rapid hemostasis, and postsurgical tissue
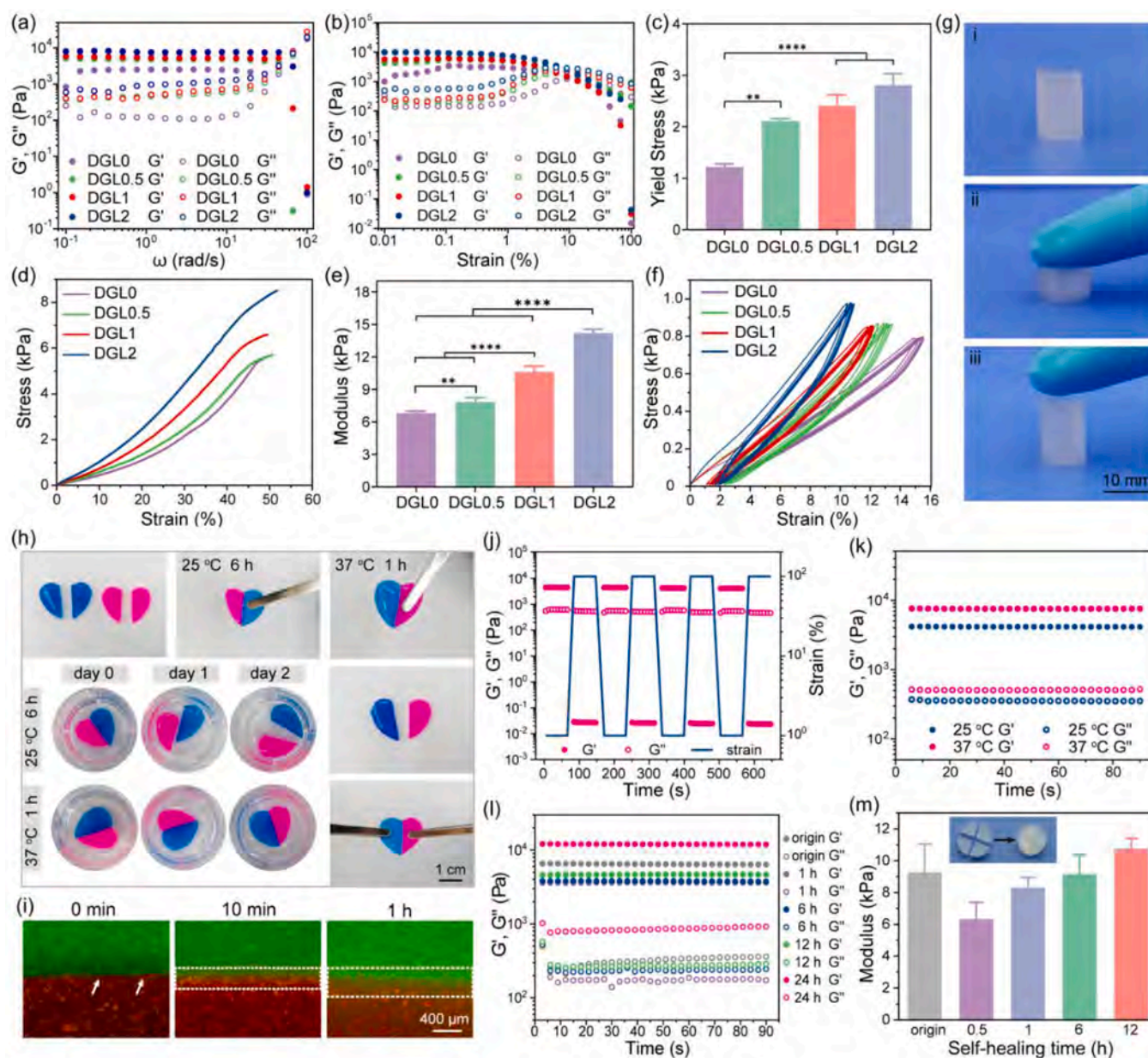
Fig. 2. Mechanical strength and self-healing properties of the DGL gel sealants: (a) Amplitude sweep measurement, (b) Strain sweep measurement, and (c) Storage moduli of the DGL sealants with different Laponite nanoclay concentrations. (d) Compressive stress-strain curves, (e) Compressive moduli, and (f) Stress-strain curves for cyclic compression of the DGL sealants with different Laponite contents. (g) Compression and shape recovery of the DGL1 gel sealant. (h) Self-healing effect of the DGL1 gel at 25 °C or 37 °C for different healing time in air or in water. (i) Inverted fluorescence images of the DGL gel boundary during healing (green: FITC-tagged gel, red: RITC-tagged gel). (j) Continuous strain amplitude cyclic tests (from 1% to 100%) at 37 °C. (k) Storage and loss moduli of the damaged DGL gel after healing at 25 °C or 37 °C for 12 h. (l) Storage and loss moduli and (m) Compressive modulus of the damaged DGL gels after healing at 37 °C for different time (inset: DGL gels before and after healing). $^{**}P < 0.01$, $^{****}P < 0.0001$.

antiadhesion for suture-less wound healing, but integrating and balancing these features still pose a great challenge.

Herein, a nano-enabled DNA supramolecular hydrogel sealant (termed DGL) is designed and demonstrate to have robust tissue adhesion, injectable and self-healing properties, rapid hemostasis, and postsurgical tissue antiadhesion. Our strategy is to impart polymerizable gelatin methacrylate and Laponite nanoclay with anisotropic surface charge distributions into the DNA matrix to build a multiple physical/chemical cross-linked network. The resulting DGL sealant has tunable and dynamic mechanical properties, achieves rapid adhesion and sealing to dynamically wet tissues, and shows rapid blood coagulation, hemostatic properties, and post-surgical antiadhesion. Furthermore, this biocompatible

supramolecular nanoenabled hydrogel sealant can fill defects, ad-here firmly to the wound surface, and promote ulcer wound healing.

Results and discussion

Preparation of DGL gels

The preparation process of the DGL hydrogel sealant is shown in Fig. 1a. DNA with a high degree of base complementary pairing is used as the main building block to construct the physically cross-linked networks, endowing the DGL hydrogel with dynamic rever-sibility *via* multiple hydrogen bonding. In addition, biocompatible and degradable methacrylate gelatin (GelMA) is imparted into the DNA matrix to construct the chemical crosslinking network for

mechanical reinforcement. The *in situ* polymerization of GelMA supposes to entangle the polymer chains and interlocks with the surface layers of tissues and the generated radicals may also react with the amine and thiol groups of tissues forming covalent bonds [29–31], leading to strong tissue adhesion. Silicate nanoclay (Laponite), a bioactive substance with both positive and negative surface charges and the capability of activating the coagulation cascade reaction and coagulation factors [32,33], is introduced to the hydrogels to promote coagulation and hemostasis. The Laponite nanoclays can further act as cross-linking points in the hydrogel to form an interconnected physical cross-linked network with both negatively phosphate groups of DNA and charged amine/carboxyl groups of GelMA through electrostatic interactions [23,34]. We further measured the zeta potential of DNA, Laponite nanoclays, GelMA and their aqueous mixture with weight ratio of 1:1:1 at pH 7.0 (Fig. S1, Supporting Information). It is shown that the zeta potential of DNA, Laponite nanoclays and GelMA is − 16.4 ± 2.1, − 41.1 ± 4.4 and 2.9 ± 0.03 mv, respectively. Notably, GelMA has an amphoteric feature and presents both negative and positive charges. The zeta potential of the mixture DGL is about 2.0 ± 1.1 mv, indicating the interactions of Laponite nanoclays with DNA and GelMA. The dispersion composed of DNA, GelMA, Laponite nanoclays, and initiator undergoes DNA unwinding and reassembly by temperature heating and cooling, subsequently forming the DNA/GelMA/Laponite (DGL) pregel.

The DGL pregel has shear-thinning properties. The DGL1 pregel with 1 wt% Laponite nanoclay is injectable by a syringe and can be shaped into the designed form, *i.e.*, "D", "N", and "A" letters (Fig. 1b and Movie S1, Supporting Information). To quantitatively characterize the shear thinning properties of the DGL pregels, a rheometer is used to measure the viscosity of the pregels with different concentrations of Laponite nanoclays at 37 °C. The viscosity decreases sharply with increasing shear rates from $0.1 \, s^{-1}$ to $100 \, s^{-1}$, but increases with Laponite concentration (Fig. S2, supporting information). Also, the viscosity of DGL pregel decreases with increasing temperature (Fig. S3, Supporting Information). Generally, a lower viscosity indicates better injectability. To investigate the effects of the crosslinking network on the injection properties, the DNA gel, DNA/Laponite (DL) gel, DGL pregel, and DGL gel (after polymerization) are tested by passing them through needles (18 G and 22 G) into PBS at different temperature (Fig. S4, Supporting Information). At a low temperature, it is difficult to maintain a stable gel after injection of the DNA gel and DL gel, resulting in discontinuous gel fragments after injection by the 22 G needles. In contrast, the DGL pregel shows good injectability and can maintain stable gelling integrity after injection. After photocuring, the DGL gel cannot pass through the 22 G needle, possibly due to the presence of additional chemically crosslinked networks. The injectability and mechanical reversibility of the hydrogels improve significantly at a higher temperature of 60 °C, indicating that the injectability of the hydrogel can be manipulated by adjusting the cross-linking network density, temperature, and needle size. The promising injectability and reversible features allow us to repeatedly process the DGL pregel and adapt it to the complex morphology of tissue defects (Fig. 1c and d). The mechanical reinforcement of additional chemical cross-linking induced by UV curing is corroborated by rheological analysis. As shown in Fig. 1e, the storage moduli (G′) of all the DGL pregels increase after UV curing. For example, the storage modulus of the DGL0 pregel is approximately 1.2 kPa and increases to 3.0 kPa for the DGL0 gel.

Supplementary material related to this article can be found online at doi:10.1016/j.nantod.2023.101825.

Mechanical and self-healing properties of the DGL gels

The mechanical strength of the DGL gels are determined on a rheometer. As shown in the frequency curve (Fig. 2a), the storage moduli of the DGL gels remain relatively stable in the frequency range (0.1–10 rad/s), with values higher than the loss moduli (G″) indicative of the gelling state of the DGL gels. Increasing the concentrations of Laponite nanoclays improves the mechanical strength of the DGL gels. This characteristic is confirmed in the strain curve and the yield stress of the DGL gels increases from 1.22 ± 0.6 kPa to 2.81 ± 0.22 kPa with increasing Laponite nanoclay concentration (Fig. 2b and c).

The compressive properties of the DGL gels with different Laponite concentrations are evaluated by compressive testing. The compressive stress-strain curves show that the DGL gels have the maximum stress when compressive deformation is approximately 45% and then the stress increases slowly due to the structural damage. As the Laponite concentration goes up, the maximum stress and toughness of the DGL gels increase gradually and the compressive modulus increases from 7.84 ± 0.39 kPa to 14.21 ± 0.35 kPa (Fig. 2d and e). The mechanical recovery properties of the DGL gels are investigated by cyclic compression tests (Figs. 2f and g, and S5, Supporting Information). The DGL gels can recover to their initial stress after multiple loading-unloading cycles. Hysteresis can be observed from the stress−strain curves of all the DGL gels, suggesting that the elastic multiple crosslinking network dissipate the energy by fracture upon external stress. The results indicate that the DGL gels have good compressive properties, fatigue resistance, and mechanical reversibility due to the combination of supramolecular interactions and covalent bond networks, and the addition of Laponite enhances the compressive strength and reduces plastic deformation of the hydrogels.

Hydrogel materials are susceptible to external forces in a dynamic environment and can possibly induce slight cracks. If repair is not in time, the defects will continue to expand and cause structural damage seriously shortening the service life of hydrogels [35]. Moreover, the pregel needs self-healing properties to maintain stable gelling after injection to avoid it from being diluted or washed away by body fluids. Whether the DGL gels can self-heal quickly after damage is hence studied. Taking the DGL1 gel as an example, although the incised gel can heal after contact for 6 h at 25 °C, the healed hydrogels are separated after incubation for one day with PBS in a shaker. In contrast, when the healing temperature is increased to 37 °C, the two hydrogels show excellent healing after contact for only 1 h. The healed DGL1 hydrogel does not separate even after 2 days and resists a certain amount of external stretching without breaking (Figs. 2h and S6, Supporting Information). In addition, healing of the hydrogel contact interface is observed by inverted fluorescence microscopy. The contact surfaces of FITC chemically-tagged DGL1 gel (green) and RITC chemically-tagged DGL1 gel (red) show obvious gaps when they first come into contact. After incubation for 10 min, the interfacial boundary of two gel pieces becomes fuzzy and the overlapping fluorescence area turns slightly yellow (Fig. 2i), which indicates the possible movements of polymer chains and gel healing at the interface. When the contacting time is prolonged to 1 h, the interfacial boundary is difficult to define, revealing the improved healing of DGL gel with increasing time.

The self-healing behavior of the DGL1 gel is determined quantitatively by rheological tests. As shown in Fig. 2j, in the strain test (1%−100% alternating cyclic strain), G′ is higher than G″ when the strain is 1%, while G′ is lower than G″ when the strain increases to 100%, indicating that the hydrogel is damaged and turns into a sol state. When the strain is reduced to 1% again, G′ and G″ can recover to the initial values. Even after multiple strain cycles, the gel can instantly recover the initial modulus value, indicating that the DGL gel has excellent self-healing properties. To further study the effects
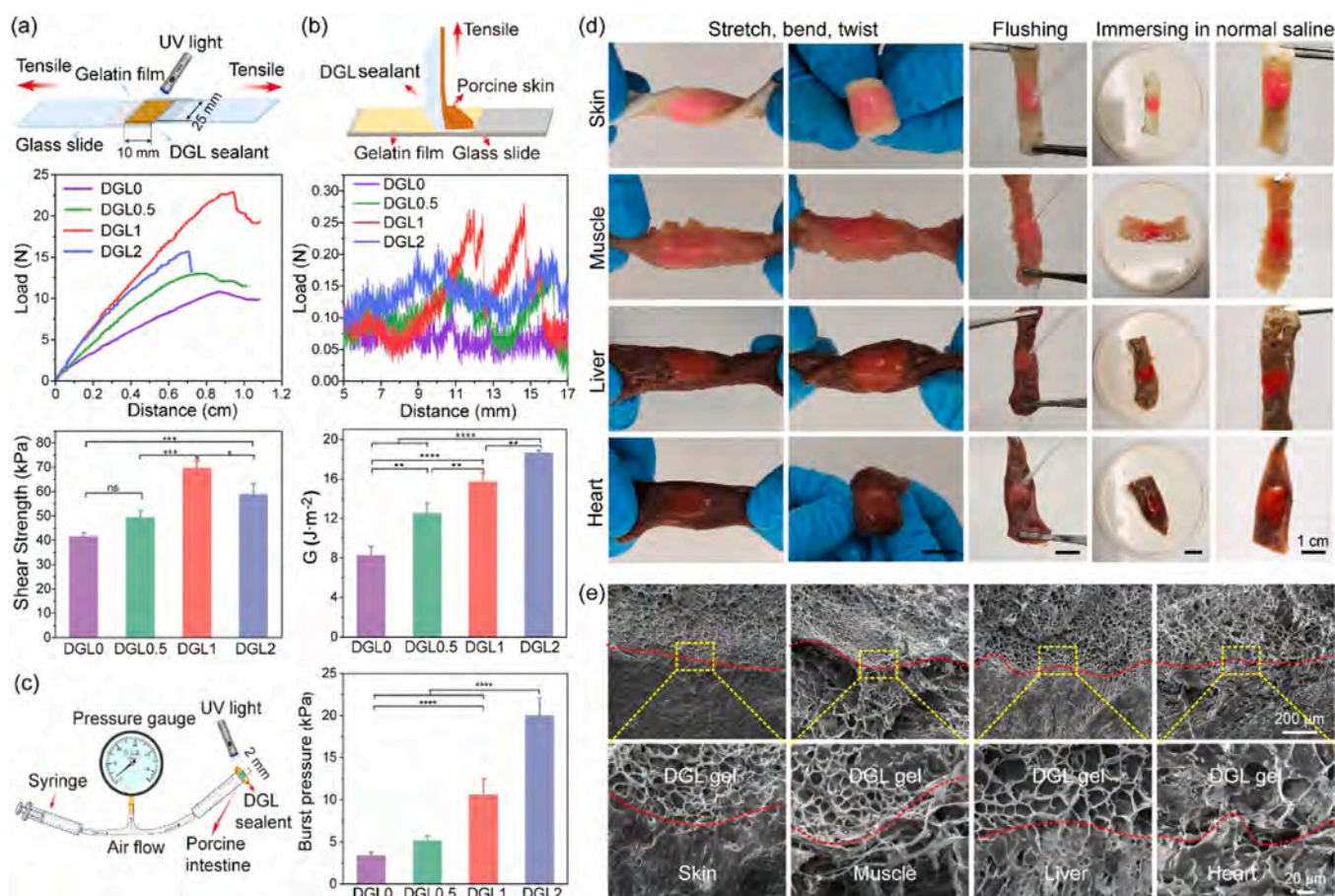
Fig. 3. Tissue adhesion properties of the DGL gel sealants: (a) Load-displacement curves and adhesive strength of the DGL sealants in lap shear test. (b) Load-displacement curves and peeling energy of porcine inner epidermis bonded with the DGL sealants on glass slides in the 90° peeling test. (c) Burst pressure test of the DGL sealants applied to porcine intestine. (d) DGL gel sealants adhering to various tissues able to withstand curling, bending and stretching while maintaining strong adhesion when subjecting to flowing water and immersing in normal saline. (e) SEM images of the DGL hydrogel sealant adhering to various tissues. $^{*}P < 0.05$, $^{**}P < 0.01$, $^{***}P < 0.001$, $^{****}P < 0.0001$.

of temperature and healing time on healing, the hydrogels are healed at different temperature for different time. The hydrogels healed at 37 °C have a higher storage modulus than those healed at 25 °C because a higher temperature favors chain movement and accelerates healing (Fig. 2k). Similarly, when the healing time is prolonged, more supramolecular moieties can be distributed at the interface of the hydrogels and the storage or loss moduli and compressive moduli increase gradually (Fig. 2l). The compressive mechanical test results in Fig. 2m demonstrate that the hydrogels separate into 4 parts and the mechanical properties recover after contact for 6–12 h. The above results indicate that the rapid self-healing properties of DGL hydrogel sealants benefit from reversible supramolecular interactions, enabling them to be repaired in time when subjected to external damage, thereby extending their service life.

Structural morphology and stability of the DGL gel sealants

The morphology of the DGL gels is examined by scanning electron microscopy (SEM). The lyophilized DGL gels show regular interconnective macroporous structures and the pore walls are smooth. The pore size is in range of 4–18 μm and the porosity is approximately 16–47% (Fig. S7, Supporting Information). The pore size and porosity decrease after addition of Laponite nanoclays, which is due to the increased cross-linking density of the DGL gels.

In the physiological environment, hydrogels are often prone to swelling due to the influence of osmotic pressure. Excessive swelling not only compromises the mechanical properties, but may also

affects surrounding tissues or nerves due to the volume expansion inducing inflammation. To explore the volume variation, the DGL1 gel is immersed in the aqueous buffer with different pH at 37 °C and the volume change is measured. Volume expansion of the DGL1 hydrogel is not obvious as a function of time and pH shows little influence on the stability (Fig. S8, Supporting Information). The DGL hydrogel reaches volume equilibrium within 24 h and the maximum volume expansion ratio (VER) is only 1.23 ± 0.06 at pH 7.4. The VER at pH 3.0 is even lower with a value of 1.15 ± 0.03, demonstrating better stability and lower swelling ratio under acidic conditions. The weight swelling ratio results are consistent with this volume swelling behaviors of DGL (Fig. S9, Supporting Information). The *in vitro* erosion behavior of DGL gels is studied by soaking the lyophilized hydrogels in PBS (Fig. S10, Supporting Information). DGL gels with Laponite nanoclay incorporation clearly show improved integrity, while DGL0 gel demonstrates obvious erosion after 7 days and completely disintegrates after 21 days. The weight retention rates of DGL0.5, DGL1 and DGL2 gels after 21 days in PBS are 41.0 ± 4.9%, 53.6 ± 11.7% and 79.4 ± 8.5%, respectively.

Tissue adhesion of DGL gel sealants

Hydrogels with good tissue adhesion properties can facilitate rapid wound closure and prevent blood exudation. The adhesion properties of the DGL hydrogel sealants are determined by lap shear tests, 90° pigskin peel tests. and burst pressure tests. Fig. 3a shows the schematic diagram and results of the lap shear of the DGL gels. The adhesive strength is correlated to the concentration of Laponite
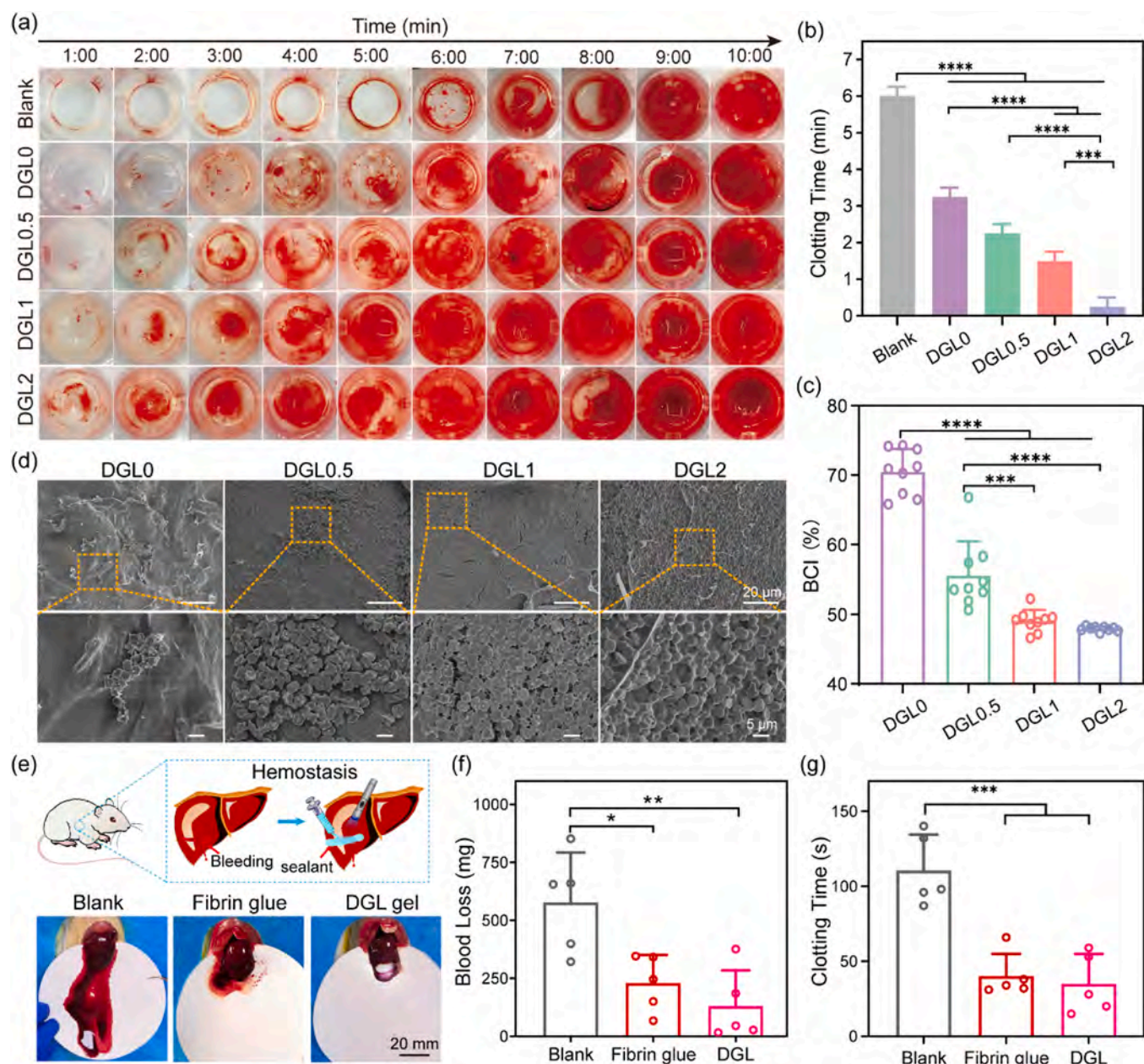
Fig. 4. *In vitro* whole blood clotting and *in vivo* hemostatic properties of the DGL sealants: (a) Blood clotting kinetics of the DGL sealants with different nanoclay contents. (b) Blood clotting time and (c) Blood clotting index. (d) SEM images of red blood cells and platelets on the DGL sealants. (e) Hemostatic effects of the DGL1 sealant and fibrin glue in the rat liver hemorrhage model. Hemostatic performance evaluated quantitatively by (f) Blood loss and (g) Hemostasis time. *$P < 0.05$, **$P < 0.01$, ***$P < 0.001$, ****$P < 0.0001$.

nanoclays and increases to 69.67 ± 2.96 kPa when the Laponite nanoclay concentration is increased to 1.0 wt%. However, when the Laponite nanoclay concentration is increased to 2.0 wt%, the adhesive strength diminishes. This may be because the high concentration of Laponite nanoclays leads to excessive crosslinking of the hydrogel matrix and limits movements of the polymer chains and interactions between the polymer chains and substrate surface. The failed interfaces of the hydrogels/glass substrates are observed after the lap shear test. As shown in Fig. S11a (Supporting Information), the DGL0 gel sealant exhibits cohesion failure due to the relatively weak mechanical strength, whereas the other DGL gel sealants containing nanoclays show different adhesion failure. The shear strengths of DGL gel sealants are higher than that of commercial fibrin glue (15.56 ± 0.77 kPa) tested in previous study [36]. To characterize the tissue adhesion of different sealants, 90° pigskin peeling tests are further performed. The results show that the

peeling energy of the DGL gels from the inner epidermis increases significantly with Laponite concentration up to 18.63 ± 0.28 J m^{-2}, and the highest peeling energy from the outer epidermis is approximately 5.03 ± 0.79 J m^{-2} (Figs. 3b and S11b-d, Supporting Information). Practically, the hydrogel sealants inevitably need to withstand a certain pressure when sealing wounds, including blood pressure and intraorgan pressure. To further characterize the ability of DGL hydrogels to seal tissues under pressure, *in vitro* burst pressure tests are performed (Fig. 3c and Movie S2, Supporting Information). The burst pressure of the DGL hydrogels on pig intestines increases from 3.38 ± 0.38 kPa to 5.15 ± 0.54 kPa, 10.56 ± 1.88 kPa and 19.98 ± 2.06 kPa for DGL0, DGL0.5, DGL1 and DGL2, respectively, suggesting that the DGL gel sealants are capable of bearing human blood pressure (10.6–16.0 kPa, 80–120 mmHg) [37].

Supplementary material related to this article can be found online at doi:10.1016/j.nantod.2023.101825.
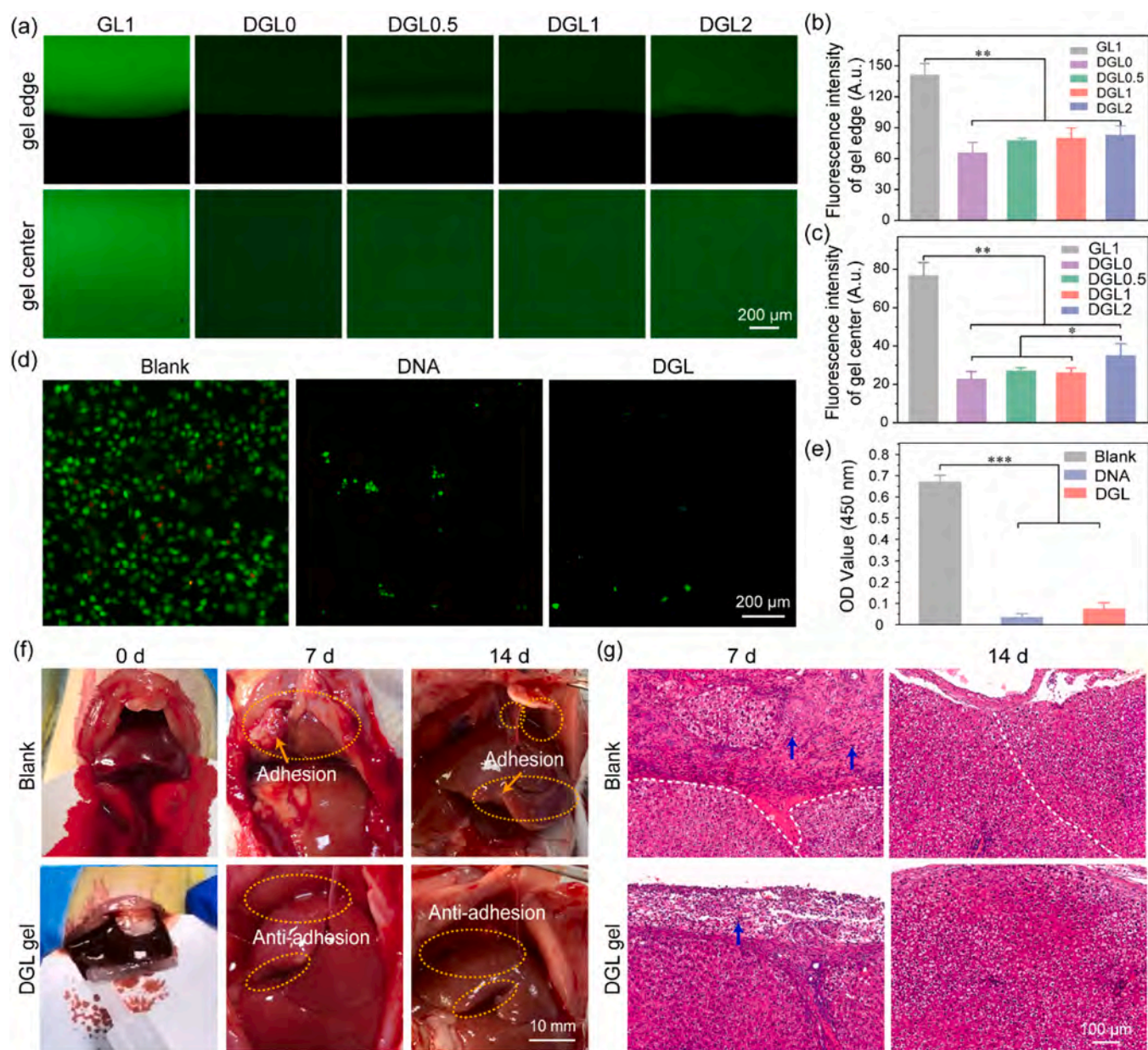
Fig. 5. Post-operative anti-adhesive properties of the DGL sealants: (a) Fluorescence images of protein adsorption of DGL gel sealants and GelMA-Laponite hydrogel (GL1) after incubation with the BSA-FITC solution. Quantitative analysis of the fluorescence intensity (b) at the edge of the hydrogels and (c) inside the hydrogels. (d) Confocal images of cell adhesion on the blank plates, DNA, and DGL1 hydrogels after culturing for 1 day. (e) Quantitative analysis of cell growth. (f) Tissue repair effect and anti-adhesion of the DGL sealant in the rat liver defect model on the 7th and 14th day after surgery. (g) Representative H&E staining images of the liver treated with the DGL sealant on the 7th and 14th day post-surgery (×100, dotted line showing the adhesion boundary and the blue arrow showing the inflammatory cells). $^{**}P < 0.01$, $^{***}P < 0.001$.

In the dynamic and wet wound environment, it is critical for the hydrogel to maintain strong adhesion to the tissue. In this regard, the DGL1 hydrogel sealant is injected into various tissues (porcine skin, muscle, liver, and heart) to form a gel after *in situ* polymerization. It is clear that the DGL1 gel sealant adheres firmly to tissues and no detachment can be observed when the tissues are twisted, bent, and stretched (Fig. 3d and Movie S3, Supporting Information). The DGL1 sealant is rinsed under rapid flowing water and there is no adhesion failure. After immersion in normal saline for 2 h, the DGL1 sealant maintains tight adhesion with tissues, demonstrating that the DGL1 sealant is suitable for the dynamic and humid environments. Notably, when the immersion time is prolonged to 7 days, the gel sealant can still firmly adhere to the porcine skin (Fig. S12, Supporting Information).

Supplementary material related to this article can be found online at doi:10.1016/j.nantod.2023.101825.

The interfacial morphology between the sealant and tissues is examined by SEM observation. As shown in Fig. 3e, there is an interpenetrating interfacial layer between the porous lyophilized DGL1 sealant and tissues and no obvious gap can be observed. In the interfacial region, the hydrogel partially penetrates the tissues, suggesting seamless contact and interactions. Inverted fluorescence microscopy confirms that the FITC-tagged DGL sealant slowly interpenetrates the PAM gel continuously increasing fluorescence diffusion as a function of time (Fig. S13, Supporting Information). Quantitative analysis of the fluorescence area shows that the fluorescence diffusion area increases to 80% within 1 h and complete penetration of the PAM gel can be observed after 4 h. Overall, these results demonstrate that the DGL gel sealants adhere tightly to wet

tissues due to covalent/noncovalent bonding of the DGL sealant with tissues and penetration of DGL polymer chains into tissues, consequently enabling rapid wound closure and prevention of wound bleeding.

In vitro and in vivo biocompatibility of the DGL gel sealants

The hemolysis experiment is carried out to evaluate the hemocompatibility of the DGL gel sealants (Fig. S14, Supporting Information). Compared to the bright red positive control group (ultrapure water), the supernatant is clear and no obvious hemolysis can be observed from the hydrogels. The hemocompatibility of the DGL sealants is quantitatively characterized by measuring the absorbance of the supernatant. The hemolysis rates of the hydrogel sealants are in the range of 0.12–1.28%, which are significantly lower than the critical and safe hemolytic ratio for biomaterials (5%) according to ISO/TR 7406 [38,39]. The cytocompatibility of the DGL gel sealants is evaluated by culturing L929 fibroblasts in the extracts of DGL sealants and cell growth and proliferation are assessed by Live/Dead staining and CCK-8 assays. The fibroblasts spread well with no observable death and the well plates are completely covered by cells on the 3rd day. The cell viability determined by the CCK8 assay reveals rapid proliferation in the culture medium (DMEM) conditioned with hydrogel extracts (Fig. S15, Supporting Information). In addition, the hematoxylin-eosin (H&E) staining shows no obvious tissue damage or acute pathological change in any of the major organs after the subcutaneous implantation of DGL1 gel for 5 days (Fig. S16, Supporting Information). Therefore, all of these results demonstrate the high biocompatibility and biosafety of the DGL gel sealants, which provide great potential for future clinical translation.

Coagulation and hemostasis properties of the DGL gel sealants

The Laponite nanoclay with good biocompatibility and coagulation properties is introduced to endow the DGL sealants with intrinsic coagulation properties. The in vitro coagulation and hemostasis abilities are studied by measuring the coagulation time of rabbit whole blood in contact with the hydrogels. As shown in Fig. 4a and b, the DGL0 sealant develops a small amount of clot at 3.25 ± 0.25 min, which is faster than that of the blank group without hydrogels (6 ± 0.25 min). This may be because the DGL0 sealant can absorb a certain amount of blood due to the fluid absorption driven by swelling and gelatin component somehow activates platelets and causes platelet aggregations [40–42]. Remarkably, with increasing Laponite concentration, the coagulation accelerates. The clotting time of the DGL2 sealant is 0.25 ± 0.25 min, which is significantly faster than those of the other groups. The excellent coagulation performance is attributed to the surface negative charges of Laponite nanoclays, which can promote platelet aggregation or activate the clotting factors [32,33,43].

The coagulation properties of the DGL sealants are determined according to the coagulation index (BCI). When the clotting ability is strong, the clot is more difficult to disperse and the absorbance is lower, resulting in a smaller BCI index [44]. The BCI of the DGL sealants decreases significantly from 70.46 ± 3.3% to 47.91 ± 0.33% with increasing Laponite concentration (Fig. 4c). After incubation for 5 min, the adsorption of erythrocytes and platelets on the sealants is observed by SEM. On the surface of the DGL0 sealant, a small amount of blood clotting is formed by platelet aggregation. With regard to the DGL0.5 sealant, the density of clotting increases and there are more red blood cells and platelets. When the Laponite concentration is increased to 1.0 wt% or 2.0 wt%, a large number of blood cells coagulate on the gel surface to form a coagulation layer (Fig. 4d). The results show that nanoclay-enabled DGL sealants can rapidly adsorb blood cells and initiate intrinsic coagulation with the

aid of abundant negative charges, effectively promoting coagulation and hemostasis.

The in vivo hemostatic properties of the DGL hydrogel sealants are evaluated using a rat liver hemostatic model. According to the aforementioned results related to the injectability, mechanical properties, and adhesion, the DGL1 gel sealant is chosen for the in vivo studies. After a 10 mm incision is made on the liver surface, the fibrin glue or DGL1 hydrogel sealant is injected as soon as blood flow stabilizes. There is massive bleeding on the filter paper in the untreated group which shows a blood mass of 577.6 ± 215.2 mg and it takes 110.6 ± 23.7 s to achieve hemostasis through its own coagulation mechanism (Fig. 4e-g and Movie S4–6, Supporting Information). On the other hand, the commercially available fibrin glue accelerates coagulation by utilizing fibrinogen and thrombin giving rise to better hemostatic properties (blood loss: 230.4 ± 121.1 mg, clotting time: 40.2 ± 14.7 s). However, fibrin glue gells slowly and can be easily diluted or washed away by blood. In this respect, the DGL1 pregel adheres quickly to the liver incision upon rapid photocuring, showing superior hemostatic properties such as reduced blood loss of 130.4 ± 153.6 mg and short hemostasis time of 35.0 ± 19.8 s, which are comparable to those of other recently developed adhesives [36]. The rapid hemostatic properties stem from intrinsic coagulation triggered by Laponite nanoclays in the DGL1 sealant.

Supplementary material related to this article can be found online at doi:10.1016/j.nantod.2023.101825.

Post-operative anti-adhesive properties of the DGL sealants

Preventing tissue adhesion after surgery is important for wound treatment. Here, in vitro protein adsorption and cell adhesion are examined on the DGL sealants. By observing the fluorescence intensity of the DGL sealants immersed in the BSA-FITC solution, green fluorescence from the edge or inside the hydrogel sealants is weak. In contrast, the GL1 (GelMA-Laponite 1 wt%) hydrogel exhibits bright fluorescence, indicating that a large amount of BSA-FITC is adsorbed on the hydrogel surface (Fig. 5a). This may be explained by the negatively charged BSA-FITC and corresponding electrostatic interactions with the positively charged amino acid segments of the GL1 hydrogel. However, the DGL hydrogel sealants with a large amount of DNA have abundant negative charges, thereby preventing physical adsorption of the BSA-FITC protein. Semi-quantitative analysis shows that the fluorescence intensity of the DGL sealants is obviously lower than that of GL1 hydrogel and it increases slightly with the concentrations of Laponite nanoclays (Fig. 5b and c). L929 cells are seeded on the DNA hydrogels and DGL sealants to study cell adhesion. After culturing for 24 h, fewer cells adhere to the DNA hydrogels and DGL sealants and most of the cells are round. The OD values of the DNA hydrogel and DGL sealant groups are considerably less than those of blank group (Fig. 5d and e), indicating that DNA reduces the adhesion of fibroblasts. The results disclose that the DGL sealant can reduce post-surgical tissue adhesion in vivo.

Intra-abdominal tissue adhesion caused by hepatectomy can produce severe pain and post-surgical complications in patients and repeated operations are not desirable[45]. A rat liver lobectomy model is utilized to study the anti-adhesion and in vivo degradation properties of the DGL sealants. A part of the right hepatic lobe of the rat is resected with a defect width of 20 mm after the hemostasis experiment and the DGL1 sealant is applied to completely cover the hepatic lobe defect (Movie S7, Supporting Information). After 7 days post-surgery, the blank groups developed severe adhesion in the abdominal cavity, including nonpeelable adhesion of the right and left liver lobes to the omentum as well as adhesion of the left side of the lower liver lobe to the underlying tissues (Fig. 5f). In contrast, the liver treated with the DGL1 hydrogel sealant shows no adhesion. The notch area is reduced and a small amount of sealant remains around
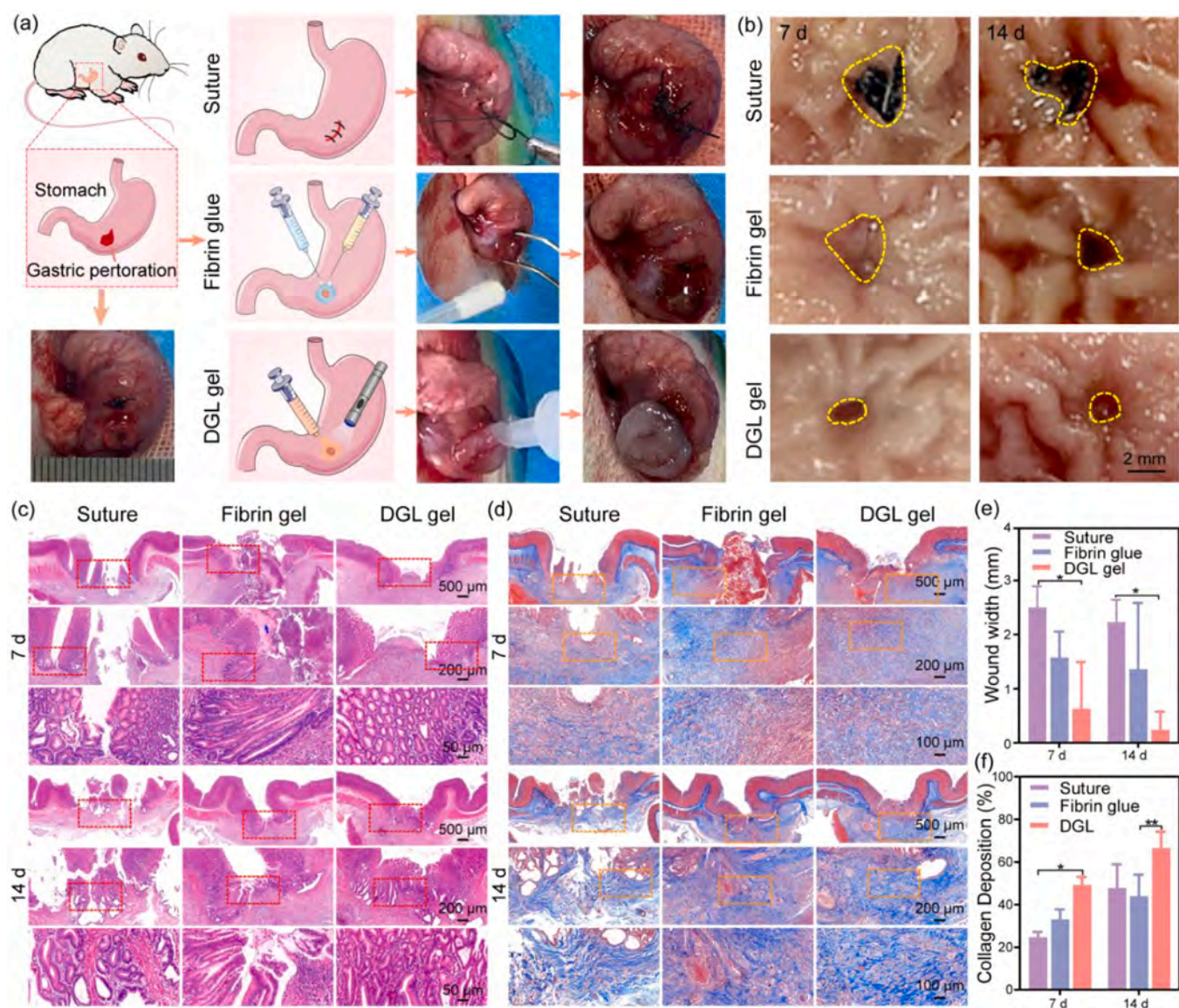
Fig. 6. Sealing and healing of rat gastric perforation wounds: (a) Schematic diagrams of the rat gastric perforation wound model, wounds sealed with sutures, fibrin glue and DGL sealant, and images of wound sealing process. (b) Images of gastric wound mucosa treated in different groups on the 7th and 14th day after surgery (dotted line representing the area of mucosal protrusion). (c) H&E staining and (d) Masson's trichrome staining images of the gastric wound slices treated in the different groups on the 7th and 14th day post-surgery (original magnifications: ×20, ×50, ×200, respectively, dotted box: magnified area). (e) Wound width and (f) Collagen deposition of gastric wounds treated in the different groups on the 7th and 14th day post-surgery. n ≥ 3, $^*P < 0.05$, $^{**}P < 0.01$.

the notch without degradation. On the 14th day, compared with the blank group, the rats treated with the DGL1 sealant shows no severe adhesion in the abdominal cavity, and the cross-sectional area of the notch decreases significantly. Furthermore, hematoxylin-eosin (H&E) staining reveals obvious adhesion of the liver defect in the blank group (adhesion to the greater omentum on the 7th day and adhesion to the lower liver lobe on the 14th day) (Fig. 5g). Obvious inflammatory cells, including neutrophils and lymphocytes are found from the adhesion sites. In contrast, the DGL1 hydrogel-sealed hepatic lobe defects exhibit no adhesion and a mild inflammatory response.

The *in vivo* biodegradability of the hydrogel sealant at the liver lobe sites is assessed by SEM. The surface of the normal liver lobes shows regularly textured protrusions and the DGL1 hydrogel sealant remains on the surface of the liver lobe on the 7th day post-surgery (Fig. S17, Supporting Information). The hydrogel has a macro-porous structure with a larger pore size and porosity compared to the original state and the hydrogel becomes thinner, indicating

degradability of DGL1 hydrogel sealant. On the 14th day post-surgery, the DGL1 sealant on the liver surface degrades further and only residual materials can be detected.

In vivo gastric perforation sealing and healing assessment

Gastrointestinal perforation often leads to severe bleeding and leakage of contents and phagocytosis of the wound by gastric juice can cause repeated wound ulcers. In this respect, a rat gastric perforation model is adopted to evaluate the potential application of the DGL hydrogel sealants with regard to gastrointestinal perforation or ulceration. A 5 mm diameter perforation is made in the gastric antrum and the gastric mucosa is turned outward at the perforation. Fig. 6a shows the size of the gastric perforation and schematic diagram of the treatment process. In the control group, nonabsorbable sutures are used to suture the gastric wall on both sides of the gastric perforation to achieve physical closure. Commercially available fibrin glue or DGL gel sealants are applied to the wound of
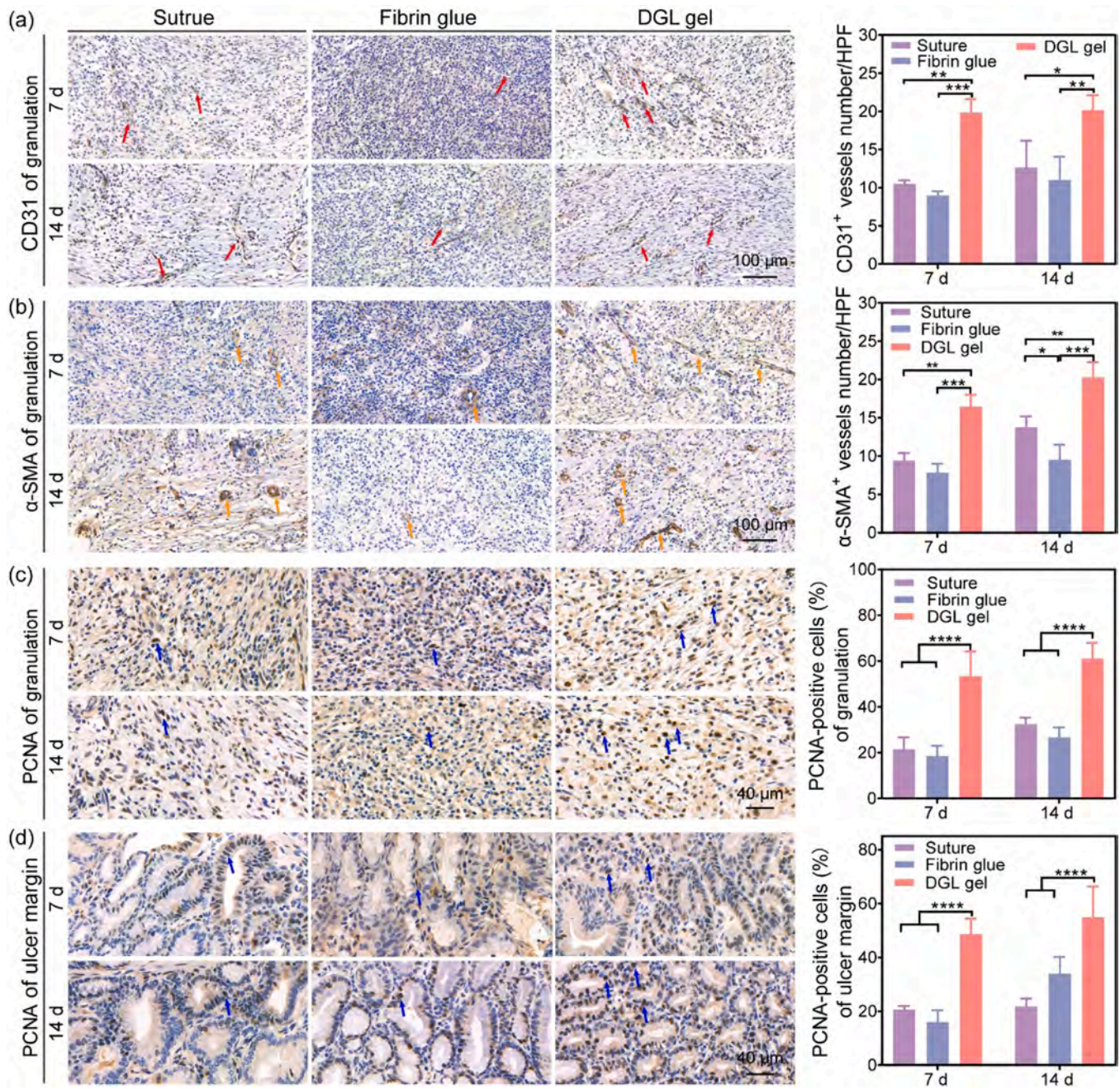
Fig. 7. Immune modulation at rat gastric perforation wounds: (a) Representative immunofluorescence images of the angiogenesis marker CD31 at the wound granulation tissue and quantification of CD31 stained blood vessels per HPF (×200, arrow: labeled blood vessel). (b) Representative images of the angiogenesis marker α-SMA at the wound granulation tissue and quantification of α-SMA stained blood vessels per HPF (×200, arrow: labeled blood vessel). (c) Representative images of PCNA staining at the wound granulation tissue and quantification of PCNA-positive cells per HPF (×400, arrow: PCNA-positive cells). (d) Representative images of PCNA staining at the ulcer margins and quantification of PCNA-positive cells per HPF (×400, arrow: PCNA-positive cells). n ≥ 3, *$P < 0.05$, **$P < 0.01$, ***$P < 0.001$, ****$P < 0.0001$.

perforation to bridge the mucosal edge of the gastric wall and seal the epigastric membrane completely (Movie S8, Supporting Information). After injection of the DGL sealant, UV light is used to initiate *in situ* gel formation for 1 min. As a result of the strong adhesion, the DGL sealant adheres firmly to the stomach wall to close the wound for rapid hemostasis and avoid leakage of contents to protect the gastric wound from gastric acid attack. As shown in the gastric defect closure diagram, the wound in the suture group shows severe bleeding after suture. The fibrin glue treatment group achieves complete sealing of the perforation, but coagulation is slower, while the DGL sealant gives rise to good sealing and rapid hemostasis. All the rats are observed for 14 days after surgery and

none shows any sign of physiological damage or systemic inflammation. On the 7th and 14th day, a layer of granulation tissue is wrapped above the epigastric wound. Although the gastric mucosal wound treated with sutures is closed, the wound area is the largest. Furthermore, the gastric mucosa of the fibrin glue and DGL sealant groups is closed completely and the bulging area of gastric mucosa treated with the DGL sealant is smaller than that of the fibrin glue group (Fig. 6b). Better repair rendered by the DGL sealant arises from strong tissue adhesion and rapid coagulation and hemostasis.

Histological analysis is performed on the gastric perforated tissue sections by H&E staining and Masson's trichrome staining on the 7th and 14th day after surgery. As shown in Fig. 6c and d, the mucosal

and serosal layers are not closed on the 7th Day for all the groups. Among them, the wound mucosal layer in the suture treatment group is damaged severely and secondary damage is observed from the surrounding tissues. The granulation tissue grows well without obvious inflammatory damage, but the collagen fibers of the granulation tissue are sparse and disordered. Significant inflammatory infiltration is observed after 7 days from the fibrin glue-treated group. Owing to infiltration of inflammation and attack by gastric juice of the mucosal lining, the gastric pit structure is destroyed (blue arrow). The granulation tissues on the gastric serosa have less collagen deposition and the collagen distribution is irregular. In addition, there is incompletely degraded fibrin glue and more inflammatory cells in the middle of the gastric perforation. In comparison, the gastric mucosa treated with the DGL sealant is close after 7 days. No obvious inflammatory infiltration is seen and there is new gastric mucosa. The density of collagen fibers in the granulation tissues is higher and the tissues are in the proliferative stage. On the 14th day, the gastric mucosa in the suture group is still severely damaged, but collagen metabolism increases. Compared to the suture group, the mucosa of the fibrin glue group shows a more obvious tendency to close, but there is still inflammatory infiltration at the contact between the granulation tissues and gastric juice, and the collagen deposition density is low. In the DGL sealant treatment group, the gastric serosal layer grows toward the center and is connected completely. The granulation tissues grow well, a large amount of collagen is deposited and arranged regularly, and the blood vessel density increases, indicating that the tissues are in the remodeling stage.

The gastric perforation repair effects are evaluated by measuring the gastric mucosal gap width (Fig. S18, Supporting Information). After different treatments for 14 days, the gastric perforation wound width of the DGL sealant group (0.23 ± 0.34 mm) is smaller than those of the suture group (2.23 ± 0.41 mm) and fibrin glue group (1.36 ± 1.23 mm) (Fig. 6e). The repair effect of the DGL sealant on gastric perforation is further evaluated by measuring the collagen deposition area in the granulation tissues. As shown in Fig. 6f, after 7 and 14 days, the collagen deposition area of the DGL sealant increases significantly compared to the suture and fibrin glue groups. Hence, the DGL sealant accelerates collagen deposition in gastric perforation and promotes wound progression from the proliferation stage to the remodeling stage to accelerate wound healing. Inflammatory infiltration of the granulation tissues is examined after gastric perforation repair by histopathological inflammation scores in gastric sections (Fig. S19, Supporting Information). Inflammatory infiltration (neutrophil and lymphocyte infiltration) of the granulation tissues above the gastric ulcer is obvious after 7 days and ameliorates after 14 days. Among them, the fibrin glue group shows the most severe inflammatory infiltration, as a lot of neutrophils, macrophages and lymphocytes are seen from the granulation tissues. In the suture group, there is a small amount of neutrophil and lymphocyte infiltration, whereas the DGL sealant group shows the fewest inflammatory cells and lowest degree of inflammatory infiltration. The results show that the DGL hydrogel sealant inhibits inflammation and promotes tissue regeneration and collagen deposition to accelerate gastric perforation wound healing.

To evaluate the effects of different treatments on gastric perforation repair, the neovascular density and cell proliferation of granulation tissues and ulcer base are evaluated by immunohistochemistry. The capillary density in the granulation tissue area is measured by immunohistochemical staining for CD31 (a marker of endothelial cells and angiogenesis) and α-smooth muscle actin (α-SMA, a marker of vascular wall smooth muscle cell differentiation). On the 7th day post-surgery, as shown in the CD31 and α-SMA staining images, the capillary density and arteriole density (arrows) in the DGL sealed granulation tissue are clearly higher than those of the suture group ($P > 0.01$) and fibrin glue group

($P > 0.001$) (Fig. 7a and b). The vascular density and vascular maturity are significantly higher after 14 days, especially the DGL sealant-treated group. In addition, the proliferating cell nuclear antigen (PCNA, a G1-S phase proliferative marker) is stained by immunohistochemistry to study the cell proliferative activity in the granulation tissues and ulcer margins. The density of the PCNA-positive cells in the DGL sealed granulation tissues is higher than those of the suture and fibrin glue groups ($P > 0.0001$) (Fig. 7c). As for the ulcer margins, in the gastric perforation samples harvested after 7 day, the density of the PCNA-positive cells in the DGL sealant group is higher than those in the other groups ($P > 0.0001$) (Fig. 7d). After 14 days, owing to complete sealing of the perforation by the fibrin glue and DGL sealant, the gastric mucosa is repaired better and the density of PCNA-positive cells increases. The density of PCNA-positive cells in the DGL sealant group remains to be greater than those of the other two groups ($P > 0.0001$). The immunohistochemical results show that treatment of gastric wounds with the DGL sealant not only promotes angiogenesis and accelerates maturation of blood vessels, but also increases the cell proliferation activity, enhances rapid proliferation of cells, and promotes healing of gastric perforation wounds.

Conclusion

A nano-enabled DNA supramolecular sealant is designed and demonstrated to promote hemostasis and wound healing in damaged soft tissues. The Laponite nanoclays combined with DNA and GelMA produce multiple physical interactions and endow the DGL sealant with unique dynamic mechanical properties. The DGL sealant has self-healing properties, tissue adhesion, low swelling ratio, and inherent hemostatic properties. The in vivo liver hemorrhage and liver injury model reveals that the DGL sealant has short hemostasis time and low blood loss, consequently reducing post-operative tissue adhesion and accelerating healing of liver injuries. In the rat gastric perforation model, the DGL sealant blocks and coagulates wounds rapidly and accelerates ulcer wound healing by reducing inflammatory infiltration and promoting angiogenesis and collagen deposition. The nano-enabled DNA supramolecular sealant described here not only reveals a promising strategy for gastric perforation repair, but also has large potential pertaining to sutureless surgical applications of other soft-tissue injuries.

Experimental Section

Materials

DNA (deoxyribonucleic acid sodium salt from herring testes, molecular weight: $\sim 6.0 \times 10^5$ Da), gelatin (from porcine skin), photoinitiator Irgacure 2959 (I2959), and methacrylic anhydride (MA) were purchased from Sigma-Aldrich. Fluorescein isothiocyanate (FITC), rhodamine B isothiocyanate (RITC), acrylamide, N,N′-methylenebisacrylamide, and glutaraldehyde were bought from Aladdin and laponite nanoclay XLG was provided by BYK-Chemie GmbH. The phosphate-buffered saline (PBS), Dulbecco's modified Eagle's medium (DMEM), fetal bovine serum (FBS) and penicillin−streptomycin solution were obtained from Life Technologies (Gibco, USA) and the Live/Dead assay kit was purchased from YESEN. The cell counting kit-8 was obtained from Tonkin Institute of Chemistry, Japan and the recombinant rat FGF-basic was purchased from PeproTech.

Preparation of DGL sealants

The Laponite nanoclay dispersion was prepared by mixing the powder with ultra-pure water and stirred for 12 h. 40 mg of DNA and a certain amount of Laponite nanoclay dispersion were dissolved in

0.8 mL of water and stirred at 40 °C for 5 h. The final mass fractions of the Laponite nanoclay were 0, 0.5 wt%, 1 wt%, and 2 wt%. 0.2 mL of the aqueous solution of GelMA (2 wt%) and I2959 (0.02 wt%) were added to the DNA/nanoclay dispersion and stirred in darkness for 5 h. The mixture was stirred vigorously at 95 °C for 3 min to unwind DNA to form a precursor solution and the precursor solution was irradiated with UV light (365 nm, 50 mW/cm^2) for 1 min [36] to obtain the DNA/GelMA/Laponite nanocomposite hydrogel sealants. The samples were denoted as DGLx, where x is 0, 0.5, 1, 2, referring to 0, 0.5 wt%, 1 wt%, and 2 wt% of Laponite nanoclay concentration, respectively. The DGL-βFGF hydrogel was prepared by adding 2 μg/mL βFGF to the precursor solution followed by curing.

The pure DNA hydrogel was prepared by dissolving DNA (4 wt%), heated to 95 °C for unwinding, and then cooled for curing. The DNA-Laponite (DL) hydrogel was prepared by a similar procedure by adding 1 wt% Laponite nanoclays. The GelMA hydrogel was formed by mixing GelMA (5 wt%) with I2959 (0.05 wt%) followed by UV polymerization. The GelMA-Laponite hydrogel (GL) was formed by imparting 1 wt% Laponite nanoclays.

Mechanical characterization

Rheological characterization

The rheological tests were performed on an ARG2 rheometer (TA Instruments). A disk-shape DGL hydrogel sample (diameter of 8 mm and thickness of 4 mm) was placed on a parallel circular plate of PP08 (8.0 mm in diameter). In the strain test, the amplitude strain range was 0.01–100%, the angular frequency was 10 rad/s, and the angular frequency varied from 0.1 rad/s to 100 rad/sin the frequency scanning test with a strain of 1%. In the time test, the frequency was kept at 10 rad/s with the strain remaining at 1%. The viscosity test was conducted at a rate of 0.1–100 s^{-1}. The strain cycle test was conducted with the strain changing alternately between 1% and 100% at a frequency of 10 rad/s. The temperature was maintained at 37 °C and the normal stress F_N was 0 N.

Mechanical strength

The compressive stress–strain of the gel sealants was tested using a dynamic mechanical analyzer (DMA Q800, USA) with a maximum compressive stress of 18 N. The cylindrical samples (diameter of 8.5 mm and thickness of 5.0 mm) were placed on clamps and the compression test was carried out by increasing the linear slope force at a rate of 0.5 N/min. The compressive modulus was calculated based on the results at 10~20% strain intervals and the toughness of the hydrogels was calculated by integrating the stress–strain curve. The cyclic compressive behavior of the DGL gels was studied using the DMA cyclic loading and unloading mode for five cycles in the range of 0–0.1 N (rate of 0.25 N/min).

Self-healing properties

The self-healing ability of the DGL hydrogels was evaluated by cutting the hydrogels into four strips which were then stained with methylene blue and rhodamine. After the hydrogel strips were kept in contact at 37 °C for 1 h, the self-healing status of the hydrogels was observed. In addition, a disc-shape DGL gel was cut, re-contacted, and incubated in a shaker (37 °C) or room temperature for a certain time. The self-healing properties as a function of time were determined by inverted fluorescence microscopy (DMILLED, Lecia, Germany) and rheological and compressive mechanical tests.

Adhesive properties

To evaluate tissue adhesion on the DGL hydrogel sealants, the lap shear test, 90° pigskin peeling test, and burst pressure test were carried out. The lap shear test was performed in accordance with the modified ASTM F2255–05 standard [29]. Two glass slides (25 mm ×

75 mm) were coated with gelatin solution (20 wt%) at 45 °C and dried overnight at ambient temperature. 100 μL of the DGL pregel were applied to a slide, covered with another slide, and pressed under a weight of 50 g. After 30 min, the sealant was cured with ultraviolet light (365 nm, 50 mW/cm^2) for 1 min. The lap shear test was performed using a texture tester (CT34500, USA). The shear strength (at the maximum shear force, F_{max}) was measured and calculated by F_{max}/S, where S is the adhesion area (n ≥ 3). The 90º pigskin peeling strength of the DGL sealants was determined by a texture analyzer. Briefly, 300 μL of the DGL pregels were applied to the inner or outer surfaces of porcine epidermis (length: 40 mm, width: 10 mm, mass approximately 2.0 g) and the hydrogel layers (20 mm × 10 mm × 1 mm) were formed after UV curing for 2 min. After incubation for 30 min in a humid environment, the DGL hydrogels were fixed on glass slides and the peeling test was carried out at a speed of 30 mm/min. According to elastic peeling theory [46], the interfacial adhesion energy was determined by G = F/d, where F is the average value of the peeling force and d is the gel width (n ≥ 3). The burst pressure test was conducted in accordance with the modified ASTM F2392–04 standard [30,47]. A piece of porcine intestine (3 cm × 3 cm) was fixed on a syringe pump and connected to a burst pressure gauge through a plastic tube. A syringe needle (18 G) was used to make a hole (diameter 2 mm) in the porcine intestinal membrane and the surface of the mesentery was kept moist. Subsequently, the DGL pregel was injected into the defect site and the sealant (diameter of 11 mm and thickness of 1.9 mm) was fixed by a rubber ring. The hydrogels were formed by rapid crosslinking by UV irradiation for 2 min. The syringe compressed the air (0.2 mL/s) until the intestinal membrane ruptured and the peak pressure was recorded as the burst pressure (n = 5).

To evaluate the dynamic wet adhesion properties of the DGL hydrogels, 200 μL of the rhodamine-stained DGL pregel were injected into fresh wet tissues (porcine skin, muscle, liver, and porcine heart) followed by curing with UV light for 1 min. Tissue adhesion was monitored after stretching, bending, twisting, and folding. The hydrogels adhering to the porcine tissues were subjected rapid water flow and then immersed in normal saline for 2 h to observe the adhesion effect in water.

The DGL pregel was also applied to porcine skin, muscle, liver, and heart. After interaction for 5 min, UV light-induced crosslinking led to the formation of the hydrogels. The tissues and DGL hydrogels were rapidly quenched and freeze-dried. The interaction of the adhesive interface between the hydrogel and tissue was examined by SEM. The DGL-FITC pregel was injected into the surface of polyacrylamide hydrogels (PAM content of 30 wt%, cross-linker *N, N'*-methylenebisacrylamide content of 0.03 wt%, initiator I2959 content of 0.5 wt%, irradiated with UV light for 5 min to cure into glue) for *in situ* solidification and incubated at 37 °C. After certain time intervals, inverted fluorescence microscopy was used to study the fluorescence penetration at the hydrogel interface and the fluorescence intensity was quantitatively analyzed by the ImageJ program.

In vivo hemostatic and postsurgical antiadhesion evaluation

The *in vivo* hemostatic properties of the DGL hydrogel sealant were determined using a liver injury model. The animal experiments were conducted according to the "Guidelines for the Care and Use of Laboratory Animals of South China University of Technology" and approved by the University Animal Ethics Committee. The SD rats (250–300 g, 7–8 weeks old, male) were anesthetized using pentobarbital sodium, placed on a 45° inclined wooden board, and wrapped in a cushioned towel to expose only the surgical site of the abdominal cavity. The abdominal cavity of the rat was incised through a 4 cm midline with a scalpel to expose the liver and then the tissue fluid near the liver was wiped gently. An incision 10 mm long and 5 mm deep was made on the hepatic lobe with a scalpel. To

form hemostatic sealing, fibrin glue or DGL sealant was injected into the incision immediately to cover the wound completely. During injection of DGL pregel, a UV lamp (365 nm, 30 mW/cm^2) was used to cure the pregel for 1 min from a distance of 5 cm. The untreated incision was the blank group. The time between sealant injection and cessation of blood exudation was recorded as the clotting time and the blood loss was calculated (n = 5).

The *in vivo* degradation properties and efficacy of post-operative adhesion prevention by the DGL hydrogel sealant were investigated at the liver injury site. The liver tissue with the hydrogel sealant related to the injury was collected for histological assessment under a microscope (Leica DM 2700 M) and digital pathology scanning system (P250 FLASH, 3D Histech) as well as SEM.

In vivo gastric perforation sealing and healing assessment

The *in vivo* sealing and tissue repair properties of the DGL hydrogel sealants were evaluated using a rat gastric perforation model. The experiment was carried out according to the Guide to the Care and Use of Experimental Animals at South China University of Technology and approved by the Animal Ethics Committee of the University. The SD rats (250–300 g, 7–8 weeks old, male) were weighed before the operation, fasted for 24 h, and were divided randomly into four groups. The abdomen of each anesthetized rat was opened with a scalpel to expose the stomach. The gastric antrum was marked with sutures. A vertical perforation 5 mm in diameter was made near the gastric antrum mark and the wound was disinfected with 2% iodophor. Two hundred microliters of fibrin glue or DGL pregel sealant was injected into the defects and then underwent UV curing for 1 min. The perforation treated with suturing was the control group. Post-operative fasting for 24 h was performed, antibiotics (penicillin potassium) were injected for 3 consecutive days, and oral antacids (omeprazole) were given for 7 consecutive days. On the 7th day and 14th day, the rats were anesthetized and weighed and stomach wound healing was studied. The tissue samples were collected and fixed with 4% paraformaldehyde, embedded into paraffin, and processed into tissue sections, which were then stained with hematoxylin and eosin (H&E) and Masson's trichrome to evaluate wound repair. The gap width of the wound and relative area of collagen deposition were calculated by ImageJ software. The histopathology of the gastric tissue sections was evaluated by calculating the numbers of neutrophils and lymphocytic infiltrates in the granulation tissue: Grade 0, no inflammatory cells; Grade 1, inflammatory infiltration of each high-power field (HPF: 400 ×) being less than 10 cells; Grade 2, inflammatory infiltration of each HPF being more than 10 cells and infiltration of wound granulation tissue being less than 50%; Grade 3, infiltrating wound granulation tissue being more than 50%.

Immunohistochemistry analysis

Immunohistochemical staining of the collected tissues was conducted to analyze the protein expression (CD31, α-SMA, and anti-proliferating cell nuclear antigen (PCNA)). The rat gastric tissue was cut into 4-μm-thick sections, deparaffinized with xylene, immersed in ethanol, and rehydrated with deionized water. Antigens were recovered using the citrate buffer solution (10 mM, pH 6.0). The endogenous peroxidase activity was inhibited by treating with hydrogen peroxide (3 wt%) for 25 min, followed by blocking the non-specific binding sites using the BSA/PBS solution (3 wt%) for 30 min. The slides were then incubated with primary antibodies (CD31 1:100, α-SMA 1:200, or PCNA 1:3000) overnight at 4 ℃. After washing with the PBS buffer, the slides were treated with the secondary antibody (goat anti-rabbit IgG (H+L), 1:1000) for 1 h and incubated with a DAB (3,3-diaminobenzidine) substrate kit (Vector Laboratories) for further color development of peroxidase. The sections were treated with hematoxylin or DAPI to stain the nuclei. The percentage of PCNA-positive cells in the granulation tissue and ulcer margins was calculated by dividing the number of DAB-positive nuclei per high-power field (400 ×) by the total number of hematoxylin-positive nuclei.

Statistical analysis

All the results were expressed as the mean ± standard deviation (SD) and statistical analysis was performed using the GraphPad Prism software. Analysis of variance (one-way ANOVA with Tukey's test) was employed to determine the statistical significance of differences. The statistical differences were defined as $*P < 0.05$, $**P < 0.01$, $***P < 0.001$, and$****P < 0.0001$, and $P < 0.05$ was considered significant.

CRediT authorship contribution statement

Manshan Xie: Investigation, Writing − original draft. **Yunhua Chen**: Conceptualization, Supervision, Writing − review & editing. **Qian Yang**: Investigation. **Qingtao Li**: Investigation. **Runlin Zhang**: Investigation. **Wenzhi Bi**: Investigation. **Yong-Guang Jia**: Methodology, Resources. **Paul K. Chu**: Writing − review & editing. **Huaiyu Wang**: Conceptualization, Writing − review & editing. **Xuetao Shi**: Conceptualization, Writing − review & editing.

Data availability

Data will be made available on request.

Declaration of Competing Interest

The authors declare that they have no known competing financial interests or personal relationships that could have appeared to influence the work reported in this paper.

Acknowledgements

Appendix A. Supporting information

Supplementary data associated with this article can be found in the online version at doi:10.1016/j.nantod.2023.101825.

References

[1] J. Rose, T.G. Weiser, P. Hider, L. Wilson, R.L. Gruen, S.W. Bickler, Estimated need for surgery worldwide based on prevalence of diseases: a modelling strategy for the WHO Global Health Estimate, Lancet Glob. Health 3 (2015) S13–S20.

[2] G.M. Taboada, K.S. Yang, M.J.N. Pereira, S.H.S. Liu, Y.S. Hu, J.M. Karp, N. Artzi, Y.H. Lee, Overcoming the translational barriers of tissue adhesives, Nat. Rev. Mater. 5 (2020) 310–329.

[3] N. Annabi, K. Yue, A. Tamayol, A. Khademhosseini, Elastic sealants for surgical applications, Eur. J. Pharm. Biopharm. 95 (2015) 27–39.

[4] A.J. Singer, L.C. Perry, R.L. Allen Jr., In vivo study of wound bursting strength and compliance of topical skin adhesives, Acad. Emerg. Med 15 (2008) 1290–1294.

[5] M.J. Larson, J.C. Bowersox, R.C. Lim, J.R. Hess, Efficacy of a fibrin hemostatic bandage in controlling hemorrhage from experimental arterial injuries, Arch. Surg. 130 (1995) 420–422.

[6] W.D. Spotnitz, Fibrin sealant: past, present, and future: a brief review, World J. Surg. 34 (2010) 632–634.

[7] H.-H. Chao, D.F. Torchiana, BioGlue: albumin/glutaraldehyde sealant in cardiac surgery, J. Card. Surg. 18 (2003) 500–503.

[8] K.D. Kim, N.M. Wright, Polyethylene glycol hydrogel spinal sealant (duraseal spinal sealant) as an adjunct to sutured dural repair in the spine results of a prospective, Multicent., Random Control. Study, Spine 36 (2011) 1906–1912.

[9] P. Slezak, A. Klang, J. Ferguson, X. Monforte, P. Schmidt, B. Bauder, A. Url, M. Osuchowski, H. Redl, D. Spazierer, H. Gulle, Tissue reactions to polyethylene glycol and glutaraldehyde-based surgical sealants in a rabbit aorta model, J. Biomater. Appl. 34 (2020) 1330–1340.

[10] P.A. Leggat, D.R. Smith, U. Kedjarune, Surgical applications of cyanoacrylate ad-hesives: a review of toxicity, ANZ J. Surg. 77 (2007) 209–213.

[11] M. Fujita, G.M. Policastro, A. Burdick, H.T. Lam, J.L. Ungerleider, R.L. Braden, D. Huang, K.G. Osborn, J.H. Omens, M.M. Madani, K.L. Christman, Preventing post-surgical cardiac adhesions with a catechol-functionalized oxime hydrogel, Nat. Commun. 12 (2021) 3764–3778.

[12] Y. Bu, L. Zhang, G. Sun, F. Sun, J. Liu, F. Yang, P. Tang, D. Wu, Tetra-PEG Based Hydrogel Sealants for In Vivo Visceral Hemostasis, Adv. Mater. 31 (2019) 1901580.

[13] B. Reid, M. Gibson, A. Singh, J. Taube, C. Furlong, M. Murcia, J. Elisseeff, PEG hydrogel degradation and the role of the surrounding tissue environment, J. Tissue Eng. Regen. Med 9 (2015) 315–318.

[14] P.J.M. Bouten, M. Zonjee, J. Bender, S.T.K. Yauw, H. van Goor, J.C.M. van Hest, R. Hoogenboom, The chemistry of tissue adhesive materials, Prog. Polym. Sci. 39 (2014) 1375–1405.

[15] W. Wang, Z. Zeng, L. Xiang, C. Liu, D. Diaz-Dussan, Z. Du, A.B. Asha, W. Yang, Y.Y. Peng, M. Pan, R. Narain, J. Liu, H. Zeng, Injectable self-healing hydrogel via biological environment-adaptive supramolecular assembly for gastric perfora-tion healing, ACS Nano 15 (2021) 9913–9923.

[16] S. Liu, D. Qi, Y. Chen, L. Teng, Y. Jia, L. Ren, Quadruple hydrogen bonds and thermo-triggered hydrophobic interactions generate dynamic hydrogels to modulate transplanted cell retention, Biomater. Sci. 7 (2019) 1286–1298.

[17] D. Zhang, G. Cai, S. Mukherjee, Y. Sun, C. Wang, B. Mai, K. Liu, C. Yang, Y. Chen, Elastic, persistently moisture-retentive, and wearable biomimetic film inspired by fetal scarless repair for promoting skin wound healing, ACS Appl. Mater. Interfaces 12 (2020) 5542–5556.

[18] R. Yu, M. Li, Z. Li, G. Pan, Y. Liang, B. Guo, Supramolecular thermo-contracting adhesive hydrogel with self-removability simultaneously enhancing noninvasive wound closure and MRSA-infected wound healing, Adv. Healthc. Mater. 11 (2022) 2102749.

[19] J. Sun, L. Xiao, B. Li, K. Zhao, Z. Wang, Y. Zhou, C. Ma, J. Li, H. Zhang, A. Herrmann, K. Liu, Genetically engineered polypeptide adhesive coacervates for surgical applications, Angew. Chem. Int. Ed. 60 (2021) 23687–23694.

[20] M. Shin, J.H. Ryu, J.P. Park, K. Kim, J.W. Yang, H. Lee, DNA/Tannic acid hybrid gel exhibiting biodegradability, extensibility, tissue adhesiveness, and hemostatic ability, Adv. Funct. Mater. 25 (2015) 1270–1278.

[21] C. Li, P. Chen, Y. Shao, X. Zhou, Y. Wu, Z. Yang, Z. Li, T. Weil, D. Liu, A writable polypeptide-DNA hydrogel with rationally designed multi-modification sites, Small 11 (2015) 1138–1143.

[22] S. Basu, S. Pacelli, A. Paul, Self-healing DNA-based injectable hydrogels with reversible covalent linkages for controlled drug delivery, Acta Biomater. 105 (2020) 159–169.

[23] S. Basu, S. Pacelli, Y. Feng, Q. Lu, J. Wang, A. Paul, Harnessing the Noncovalent Interactions of DNA Backbone with 2D Silicate Nanodisks To Fabricate Injectable Therapeutic Hydrogels, ACS Nano 12 (2018) 9866–9880.

[24] Y. Wei, K. Wang, S. Luo, F. Li, X. Zuo, C. Fan, Q. Li, Programmable DNA hydrogels as artificial extracellular matrix, Small 18 (2022) 2107640.

[25] C. Yao, H. Tang, W. Wu, J. Tang, W. Guo, D. Luo, D. Yang, Double Rolling Circle Amplification Generates Physically Cross-Linked DNA Network for Stem Cell Fishing, J. Am. Chem. Soc. 142 (2020) 3422–3429.

[26] M.A. Shahbazi, T. Bauleth-Ramos, H.A. Santos, DNA hydrogel assemblies: brid-ging synthesis principles to biomedical applications, Adv. Ther. -Ger. 1 (2018) 1800042.

[27] Y. Zhang, J. Tu, D. Wang, H. Zhu, S.K. Maity, X. Qu, B. Bogaert, H. Pei, H. Zhang, Programmable and Multifunctional DNA-Based Materials for Biomedical Applications, Adv. Mater. 30 (2018) 1703658.

[28] C.S. Shin, F.J. Cabrera, R. Lee, J. Kim, R. Ammassam Veettil, M. Zaheer, A. Adumbumkulath, K. Mhatre, P.M. Ajayan, S.A. Curley, B.G. Scott, G. Acharya, 3D-bioprinted inflammation modulating polymer scaffolds for soft tissue repair, Adv. Mater. 33 (2020) 2003778.

[29] N. Annabi, D. Rana, E. Shirzaei Sani, R. Portillo-Lara, J.L. Gifford, M.M. Fares, S.M. Mithieux, A.S. Weiss, Engineering a sprayable and elastic hydrogel adhesive with antimicrobial properties for wound healing, Biomaterials 139 (2017) 229–243.

[30] E. Shirzaei Sani, A. Kheirkhah, D. Rana, Z. Sun, W. Foulsham, A. Sheikhi, A. Khademhosseini, R. Dana, N. Annabi, Sutureless repair of corneal injuries using naturally derived bioadhesive hydrogels, Sci. Adv. 5 (2019) eaav1281.

[31] M. Tavafoghi, A. Sheikhi, R. Tutar, J. Jahangiry, A. Baidya, R. Haghniaz, A. Khademhosseini, Engineering tough, injectable, naturally derived, bioadhe-sive composite hydrogels, Adv. Healthc. Mater. 9 (2020) 1901722.

[32] J.I. Dawson, R.O.C. Oreffo, Clay: new opportunities for tissue regeneration and biomaterial design, Adv. Mater. 25 (2013) 4069–4086.

[33] A.K. Gaharwar, R.K. Avery, A. Assmann, A. Paul, G.H. McKinley, A. Khademhosseini, B.D. Olsen, Shear-thinning nanocomposite hydrogels for the treatment of hemorrhage, ACS Nano 8 (2014) 9833–9842.

[34] J.R. Xavier, T. Thakur, P. Desai, M.K. Jaiswal, N. Sears, E. Cosgriff-Hernandez, R. Kaunas, A.K. Gaharwar, Bioactive nanoengineered hydrogels for bone tissue engineering: a growth-factor-free approach, ACS Nano 9 (2015) 3109–3118.

[35] S. Talebian, M. Mehrali, N. Taebnia, C.P. Pennisi, F.B. Kadumudi, J. Foroughi, M. Hasany, M. Nikkhah, M. Akbari, G. Orive, A. Dolatshahi-Pirouz, Self-healing hydrogels: the next paradigm shift in tissue engineering? Adv. Sci. 6 (2019) 1801664.

[36] Y. Ma, J. Yao, Q. Liu, T. Han, J. Zhao, X. Ma, Y. Tong, G. Jin, K. Qu, B. Li, F. Xu, Liquid bandage harvests robust adhesive, hemostatic, and antibacterial performances as a first-aid tissue adhesive, Adv. Funct. Mater. 30 (2020) 2001820.

[37] E.Y. Jeon, J. Lee, B.J. Kim, K.I. Joo, K.H. Kim, G. Lim, H.J. Cha, Bio-inspired swellable hydrogel-forming double-layered adhesive microneedle protein patch for re-generative internal/external surgical closure, Biomaterials 222 (2019) 119439.

[38] N. Golafshan, R. Rezahasani, M. Tarkesh Esfahani, M. Kharazizha, S.N. Khorasani, Nanohybrid hydrogels of laponite: PVA-Alginate as a potential wound healing material, Carbohydr. Polym. 176 (2017) 392–401.

[39] Y. Wang, Y. Wu, L. Long, L. Yang, D. Fu, C. Hu, Q. Kong, Y. Wang, Inflammation-responsive drug-loaded hydrogels with sequential hemostasis, antibacterial, and anti-inflammatory behavior for chronically infected diabetic wound treatment, ACS Appl. Mater. Interfaces 13 (2021) 33584–33599.

[40] Z. Zhang, G. Kuang, S. Zong, S. Liu, H. Xiao, X. Chen, D. Zhou, Y. Huang, Sandwich-like fibers/sponge composite combining chemotherapy and hemostasis for ef-ficient postoperative prevention of tumor recurrence and metastasis, Adv. Mater. 30 (2018) 1803217.

[41] X. Xie, D. Li, Y. Chen, Y. Shen, F. Yu, W. Wang, Z. Yuan, Y. Morsi, J. Wu, X. Mo, Conjugate Electrospun 3D Gelatin Nanofiber Sponge for Rapid Hemostasis, Adv. Healthc. Mater. 10 (2021) 2170095.

[42] Q. Chen, H. Yang, Y. Li, X. Wang, L. Wei, Y. Du, Effects of Yak skin gelatin on platelet activation, Food Funct. 10 (2019) 3379–3385.

[43] R.K. Avery, H. Albadawi, M. Akbari, Y.S. Zhang, M.J. Duggan, D.V. Sahani, B.D. Olsen, A. Khademhosseini, R. Oklu, An injectable shear-thinning biomaterial for endovascular embolization, Sci. Transl. Med. 8 (2016) 365ra156.

[44] N. Rajabi, M. Kharaziha, R. Emadi, A. Zarrabi, H. Mokhtari, S. Salehi, An adhesive and injectable nanocomposite hydrogel of thiolated gelatin/gelatin methacry-late/Laponite® as a potential surgical sealant, J. Colloid Interface Sci. 564 (2020) 155–169.

[45] E. Zhang, B. Song, Y. Shi, H. Zhu, X. Han, H. Du, C. Yang, Z. Cao, Fouling-resistant zwitterionic polymers for complete prevention of postoperative adhesion, Proc. Natl. Acad. Sci. 117 (2020) 32046–32055.

[46] K. Kendall, Thin-film Peeling-the Elastic Term, J. Phys. D. 8 (1975) 1449–1452.

[47] P. The International Commission on Non-Ionizing Radiation, Guidelines on Limits of Exposure to Ultraviolet Radiation of Wavelengths Between 180 nm and 400 nm (incoherent optical radiation), Healthc. Phys. 87 (2004) 171–186.

Supporting information

Nano-enabled DNA supramolecular sealant for soft tissue surgical applications

Manshan Xie,[1] Yunhua Chen,[1,2,3,4,*] Qian Yang,[1] Qingtao Li,[5] Runlin Zhang,[1,2]

Wenzhi Bi,[1] Yong-Guang Jia,[1,2] Paul K. Chu,[6] Huaiyu Wang,[7,*] Xuetao Shi[1,2,3,4,*]

[1] National Engineering Research Center for Tissue Restoration and Reconstruction, South China University of Technology, Guangzhou 510006, China

[2] School of Materials Science and Engineering, South China University of Technology, Guangzhou 510641, China

[3] Key Laboratory of Biomedical Materials and Engineering of the Ministry of Education, South China University of Technology, Guangzhou 510006, China

[4] Key Laboratory of Biomedical Engineering of Guangdong Province, and Innovation Center for Tissue Restoration and Reconstruction, South China University of Technology, Guangzhou 510006, China

[5] School of Medicine, South China University of Technology, Guangzhou 510006, China

[6] Department of Physics, Department of Materials Science and Engineering, and

Department of Biomedical Engineering, City University of Hong Kong, Tat Chee Avenue, Kowloon, Hong Kong, China

[7] Center for Human Tissues and Organs Degeneration, Shenzhen Institutes of Advanced Technology, Chinese Academy of Sciences, Shenzhen 518055, China

[*] E-mail: msyhchen@scut.edu.cn (Y.H. Chen); hy.wang1@siat.ac.cn (H.Y. Wang); shxt@scut.edu.cn (X.T. Shi)

1. Synthesis of gelatin methacrylate and fluorescence-tagged GelMA

Gelatin methacryloyl (GelMA), GelMA-FITC, and GelMA-RITC were prepared according to the methods described previously [1, 2]. The grafting rate of methacrylamide on gelatin is about 82.47% as determined by ^{1}H NMR. GelMA (1.2 g) was dissolved in 60 mL of 0.1 M NaHCO$_3$ (pH 9.0). The FITC/RITC-DMSO solution (3 mL, 10 mg/mL) was added dropwise to the GelMA solution and reacted for 1 h. The mixture was then dialyzed for 3 days against the DMSO-water mixture and deionized water (molecular weight cut-off 14 kDa). The GelMA-FITC and GelMA-RITC polymers were obtained by freeze-drying.

2. Morphology

The internal microstructure of the DGL gels was examined by scanning electron microscope (SEM, Q25, FEI, USA). The samples were washed three times with PBS, lyophilized, and gold-coated. The average pore size and porosity were determined by the ImageJ program.

3. pH stability

The pH stability of the hydrogels was assessed by immersing the samples in simulated body fluids with different pH, including simulated gastric juice (pH = 3), simulated ulcerative enteritis intestinal juice (pH = 5.5), and simulated body fluid (pH = 7.4). The rate of volume change of the DGL hydrogels was calculated by the

following equation: (v/v%) = (V_1 - V_0) / V_0 × 100%, where V_0 is the original volume of DGL hydrogels and V_1 is the volume of DGL hydrogel after soaking in the above-mentioned simulating solution.

4. *In vitro* degradation

To monitor the *in vitro* degradation characteristics of the hydrogel sealants, purified DGL hydrogels with different nanoclay concentrations were lyophilized and the dry weight was recorded (W_d). The dried hydrogel was soaked in PBS (pH = 7.4) at 37 °C. At the predetermined time, the degraded hydrogels were collected and rinsed with PBS three times to remove excess salts. The samples were freeze-dried and weighed (W_r). The remaining weight ratio was calculated by: W_r / W_d × 100%.

5. *In vitro* coagulation

The coagulation activity of the DGL sealants was determined using rabbit whole blood (anticoagulated with sodium citrate). The DGL hydrogels (200 μL) were prepared by *in situ* polymerization on a 48-well plate and the whole blood (190 μL) and 0.2 M $CaCl_2$ solution (10 μL) preheated at 37 °C were gently poured onto the hydrogels. After incubation at 37 °C for a certain time, 1 mL of PBS was added gently three times to remove the uncoagulated blood. Clot formation was monitored every 15 seconds and the clotting time was recorded. The well without hydrogel sample is served as the blank group. After incubation for 5 min, the DGL hydrogels with blood clots were

immediately soaked with 2.5% glutaraldehyde for 2 h to fix cells. The distribution of erythrocytes and platelets on the hydrogels was observed by scanning electron microscopy (MERLIN, Carl Zeiss, Germany).

The coagulation characteristics of the DGL sealants were quantitatively determined based on the blood coagulation index (BCI). Briefly, 20 mg of the DGL sealant were added into a 1.5 mL EP tube preheated on a shaker (60 rpm) at 37 °C. The rabbit whole blood (19 µL) and 0.2 M $CaCl_2$ solution (1 µL) pre-heated to 37 °C were added to the EP tube and incubated for 10 min. The blank EP tube (containing 1 µL of $CaCl_2$ and 19 µL of rabbit whole blood) without the hydrogel sealant was the blank. Ultrapure water (1 mL) was added dropwise and after centrifugation at 800 rpm for 30 s, 100 µL of the supernatant were collected and diluted four times with ultrapure water. The absorbance was monitored at 540 nm on the enzyme labeling instrument (Varioskan Flash 3001, Thermo, Finland) and the BCI was calculated according to the following equation: $BCI = A_{sample} / A_{blank} \times 100\%$, where A_{sample} and A_{blank} represent the absorbances of the sample and blank at different time points, respectively.

6. *In vitro* and *in vivo* biocompatibility

The biocompatibility of the DGL hydrogel sealants was studied using mouse epithelioid fibroblasts L929. The cells were cultured in Eagle's medium (DMEM) with 1% (v/v) penicillin-streptomycin and 10% (v/v) fetal bovine serum (FBS) solution in a humidified atmosphere with 5% CO_2 at 37 ºC. The purified disc-shaped DGL hydrogel samples (200 mg) were incubated in 10 mL of DMEM at 37 °C for 24 h. The DGL

hydrogel extract with a concentration of 20 mg/mL was obtained. L929 cells (density: 2 $\times 10^4$ cells/mL) were then inoculated on a 48-well plate and after culturing for 12 hours, DMEM was replaced by the DGL hydrogel extract and the extract was changed every other day. The cytotoxicity was determined by the Cell Counting Kit-8 (CCK-8, Dojindo).

The blood compatibility of the DGL hydrogels was evaluated by hemolysis test. 20 mg of the DGL hydrogel were immersed in saline at 37 °C and the rabbit whole blood was diluted with saline (4:5). 20 μL of the diluted blood were added to the hydrogel samples and incubated at 37 °C. The supernatant was centrifuged. The positive control group was ultrapure water (1 mL) and the negative control group was normal saline (1 mL). The absorbance at 540 nm was monitored on the enzyme labeling instrument. The hemolysis rate (H_R) was calculated as follows: $H_R = (A_S - A_N) / (A_P - A_N) \times 100\%$, where A_S, A_P and A_N are the absorbance of supernatant, positive control and negative control, respectively.

The in vivo biocompatibility of the DGL sealant was examined using Sprague Dawley rats (250-300 g, 7-8 weeks old, male). The rats were anesthetized with pentobarbital sodium. Subcutaneous incision with about 10 mm length was made at the back of rats with a scalpel. DGL1 pregel (n=3) was injected, a UV lamp (365 nm, 30 mW/cm^2) was used to cure the pregel for 1 min from a distance of 5 cm. After 5 days, the rats were then euthanized, and the major organs (heart, liver, spleen, lung, and kidney) were harvested, embedded in paraffin, sectioned and stained with H&E for histological analysis.

7. Protein adsorption

The DGL hydrogels and GelMA-Laponite hydrogel were washed with PBS and immersed in the 0.1 mg/mL fluorescein isothiocyanate-labeled bovine serum albumin (BSA-FITC) solution in a shaker for 3 h. The hydrogels were rinsed with PBS three times to remove free proteins from the surface and observed under an inverted fluorescence microscope at an excitation wavelength of 488 nm. The fluorescence intensity was analyzed semi-quantitatively by ImageJ.

8. Anti-cell adhesion

L929 cells were used to investigate anti-cell adhesion on the DGL hydrogel. 200 mg of the pure DNA hydrogel and DGL1 hydrogel sealant were immersed in the DMEM medium for 12 h. L929 cells were cultured on the surface of blank well plate, pure DNA hydrogel, and DGL1 hydrogel sealant with a seeding density of 4×10^4 cells/mL. After culturing in a constant temperature incubator for 24 h, the cell activity was assessed using the CCK-8 kit. The cell viability and adhesion were determined using a live-dead staining kit. After incubation with calcein AM/PI for 30 min, cell adhesion was observed by laser scanning confocal microscopy.
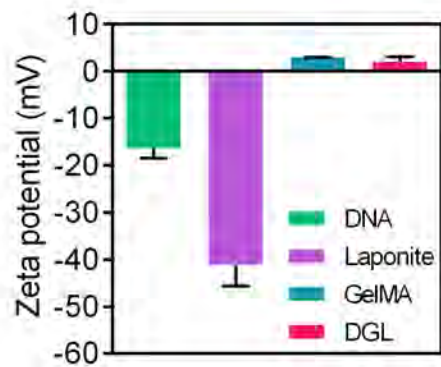
Fig. S1. Zeta potential of DNA, Laponite nanoclays, GelMA and the mixture DGL at pH 7.0.
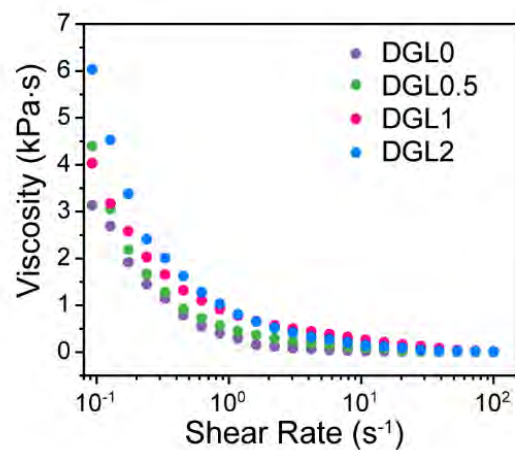
Fig. S2. Shear thinning behavior of the DGL pre-gels with different Laponite concentrations.
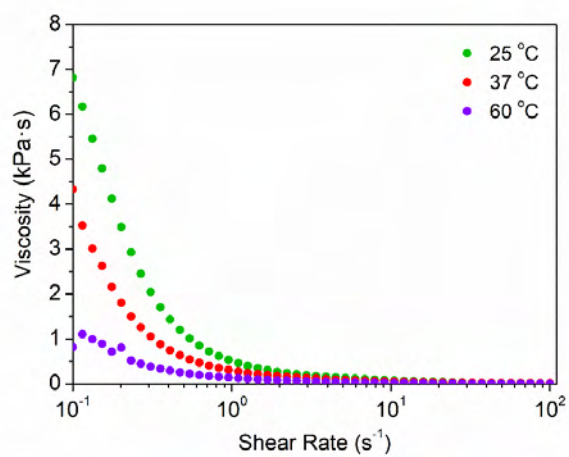
Fig. S3. The temperature dependent viscosity profiles of DGL1 pregel.
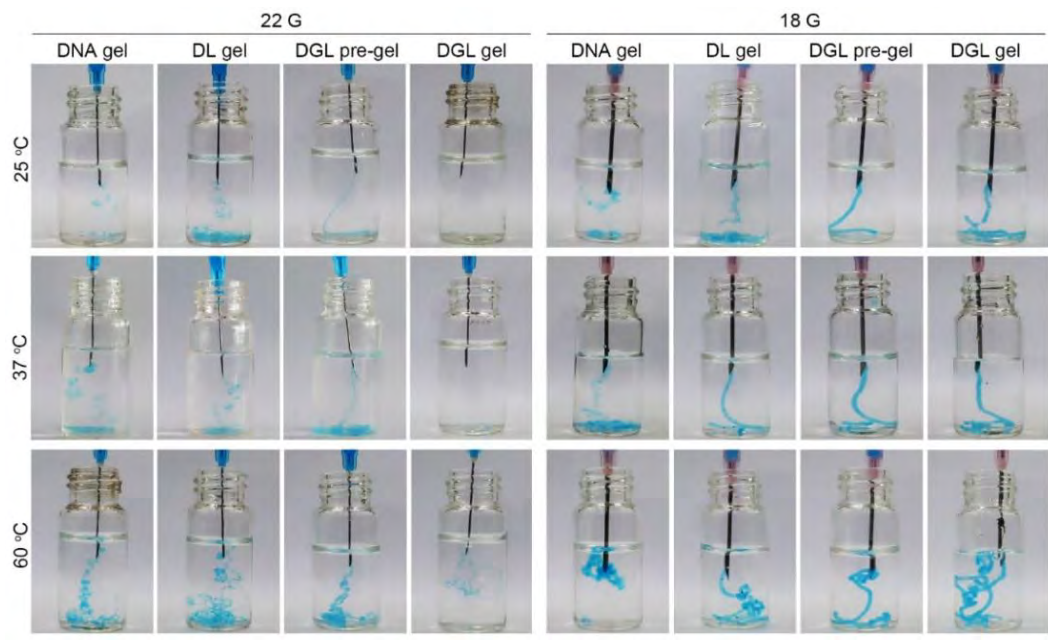
Fig. S4. Macroscopic images of the DGL gel, DL gel, DGL pre-gel, and DGL gel after injection using 22G and 18G needles into PBS at 25 ºC, 37 ºC, and 60 ºC.
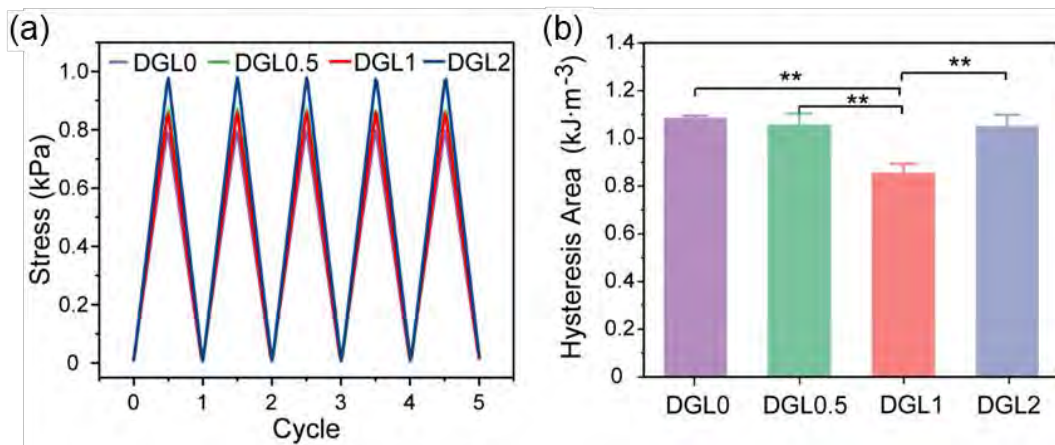
Fig. S5. (a) Stress recovery and (b) Average energy dissipation during cyclic compression of the DGL gel sealants with different Laponite concentrations.
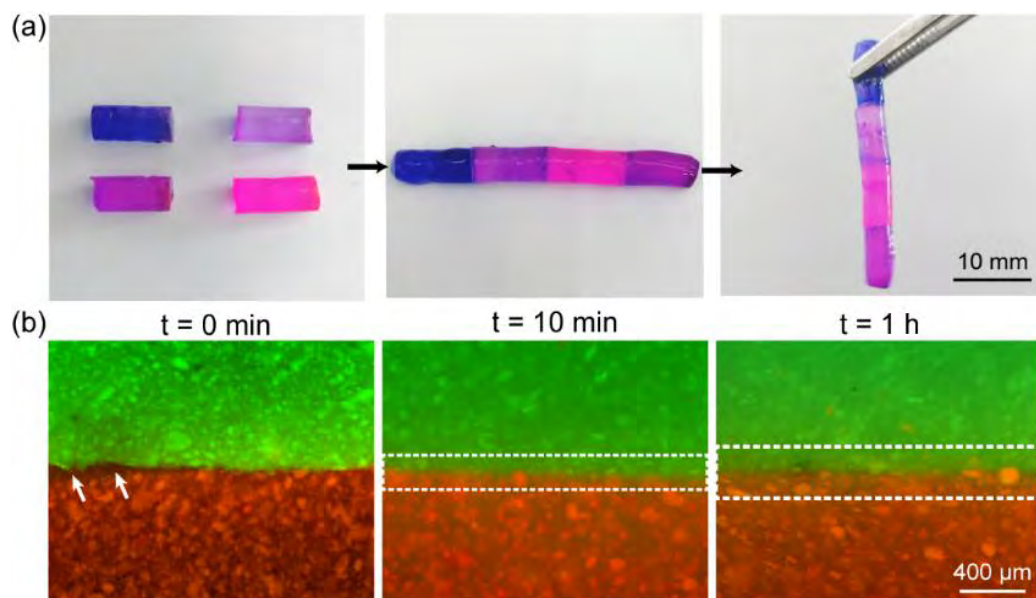
Fig. S6. (a) Self-healed DGL1 gel cylinders (stained with methylene blue and rhodamine) carrying their own weights and (b) Inverted fluorescence images of the healing boundary changes of the DGL1 hydrogel in PBS as a function of time (green: DGL1-FITC gel, red: DGL1-RITC gel, arrow: unhealed gap, virtual frame: healed area).
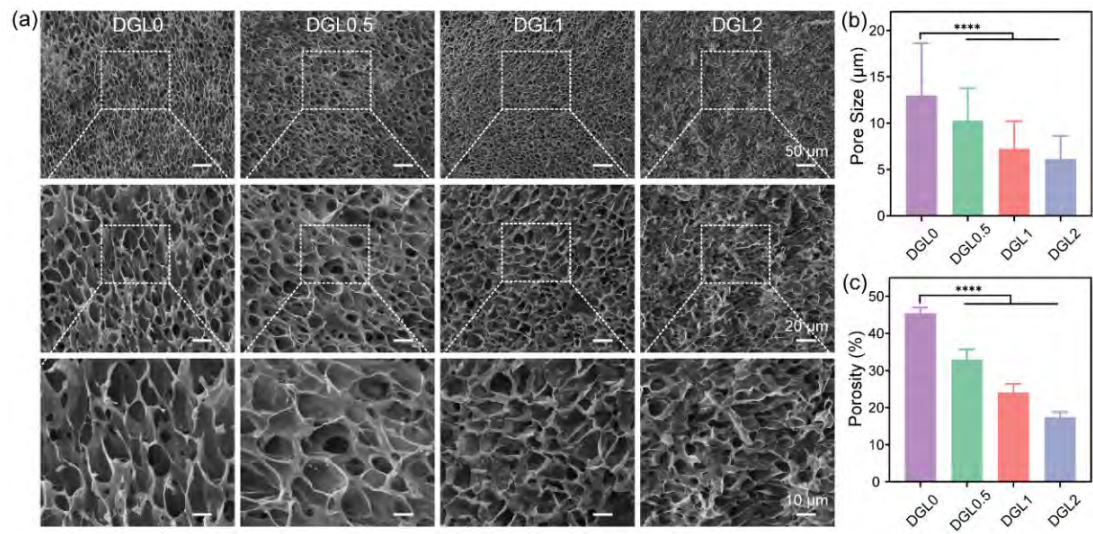
Fig. S7. Morphology of the DGL sealants: (a) SEM images, (b) Pore size, and (c) Porosity of the DGL gels with different Laponite concentrations after lyophilization (****$P < 0.0001$).
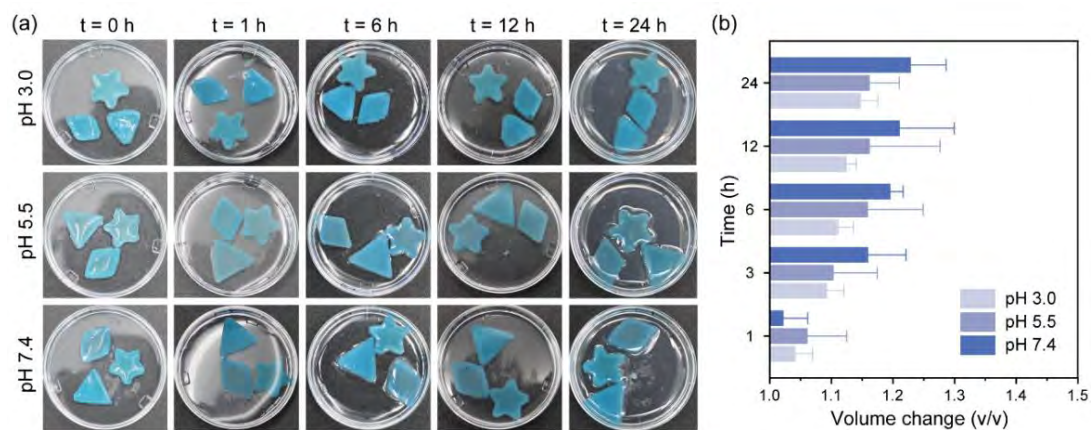
Fig. S8. Stability of the DGL sealants: (a) Stability of the DGL1 gels in simulated liquids with different pH and (b) Quantitative analysis of the volume change of DGL1 gels at different pH.
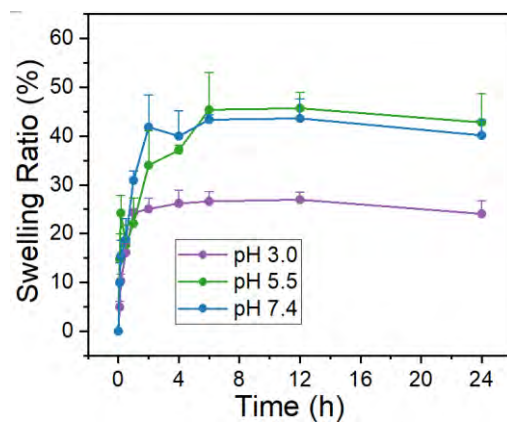
Fig. S9. The swelling ratios in weight of DGL1 gel at different pH.
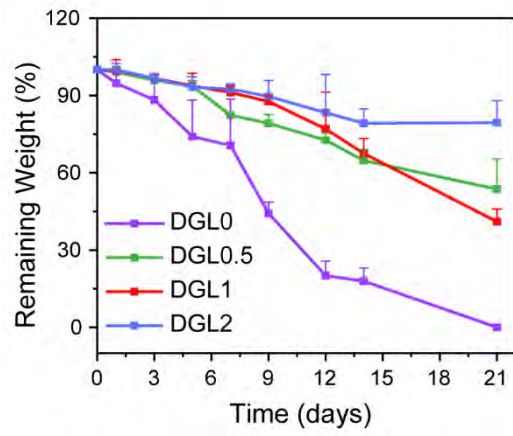
Fig. S10. Erosion of the DGL gels with different Laponite concentrations in the PBS buffer.
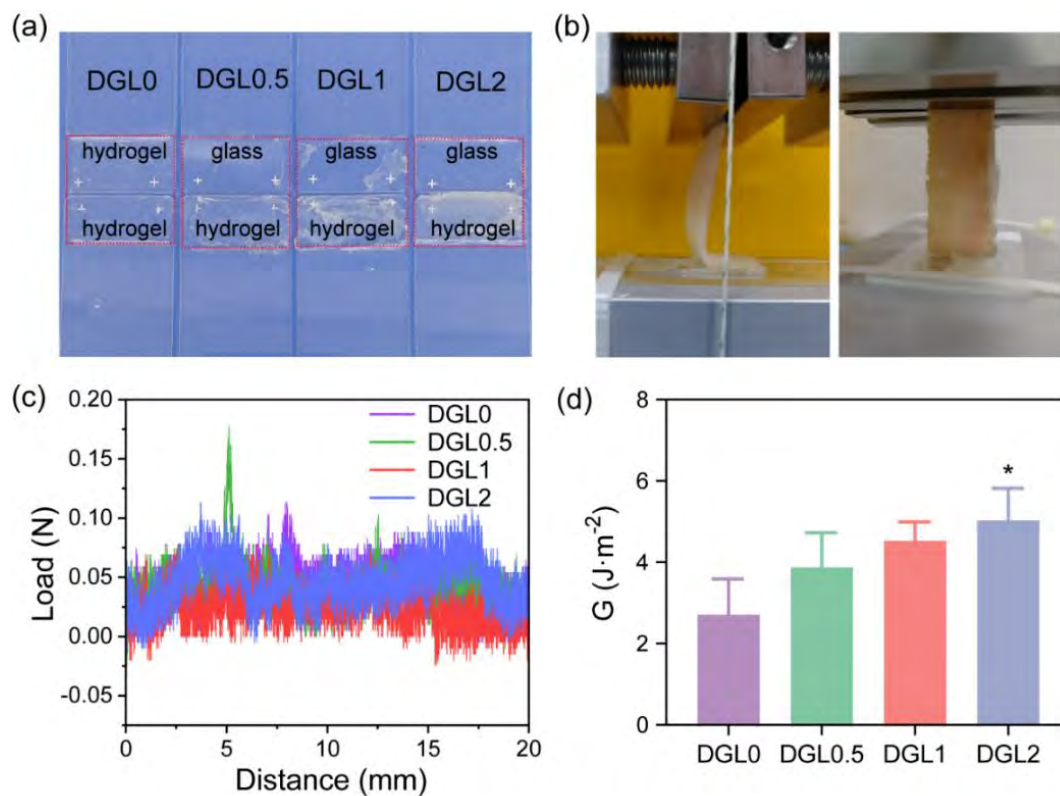
Fig. S11. (a) Comparison of the failed interfaces of DGL gels with different nanoclay contents after the lap shear test, (b) Pictures showing physical peeling and failed interface of pigskin adhered by the DGL1 gel in the 90º peeling test, (c) Displacement-force curve, and (d) Peeling energy of the DGL gels in 90º peeling test of porcine outer epidermis (*$P < 0.05$).
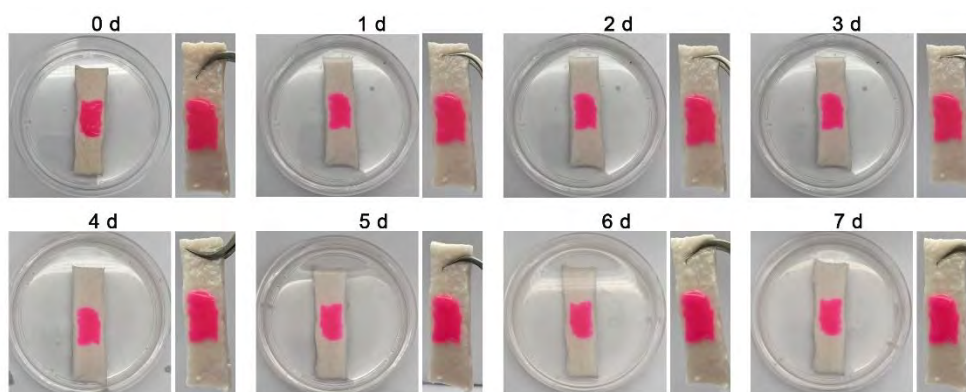
Fig. S12. DGL gel sealant keeps firm adhesion to porcine skin after immersing in normal saline for 7 days.
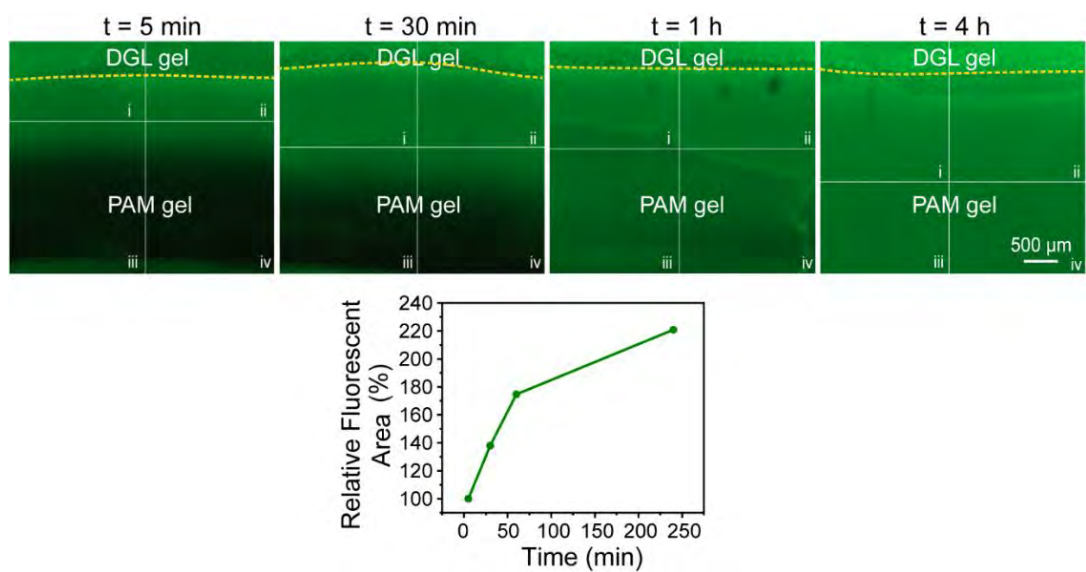
Fig. S13. Inverted fluorescence image of the FTIC-tagged DGL1 gel adhered to the PAM hydrogel with the polymer chains gradually migrating to the interior of the PAM hydrogel as a function of time.
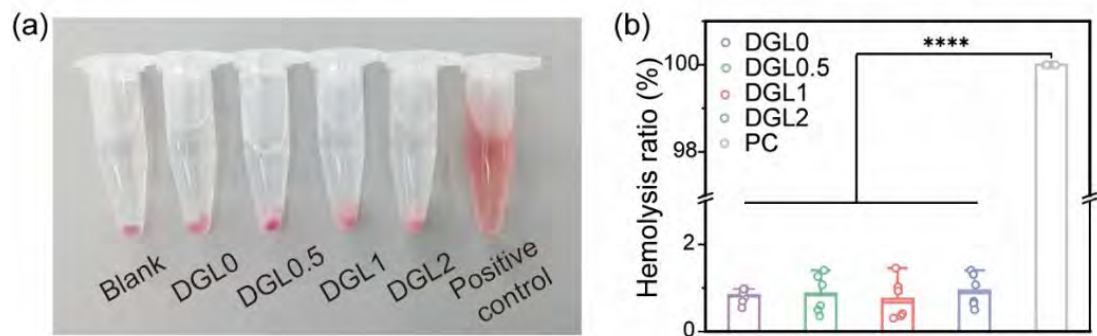
Fig. S14. Hemolysis assessment of the DGL gels: (a) Photograph after the hemolysis tests also showing the normal saline (blank), and ultrapure water (positive control) and (b) Hemolysis ratios of the DGL gels.
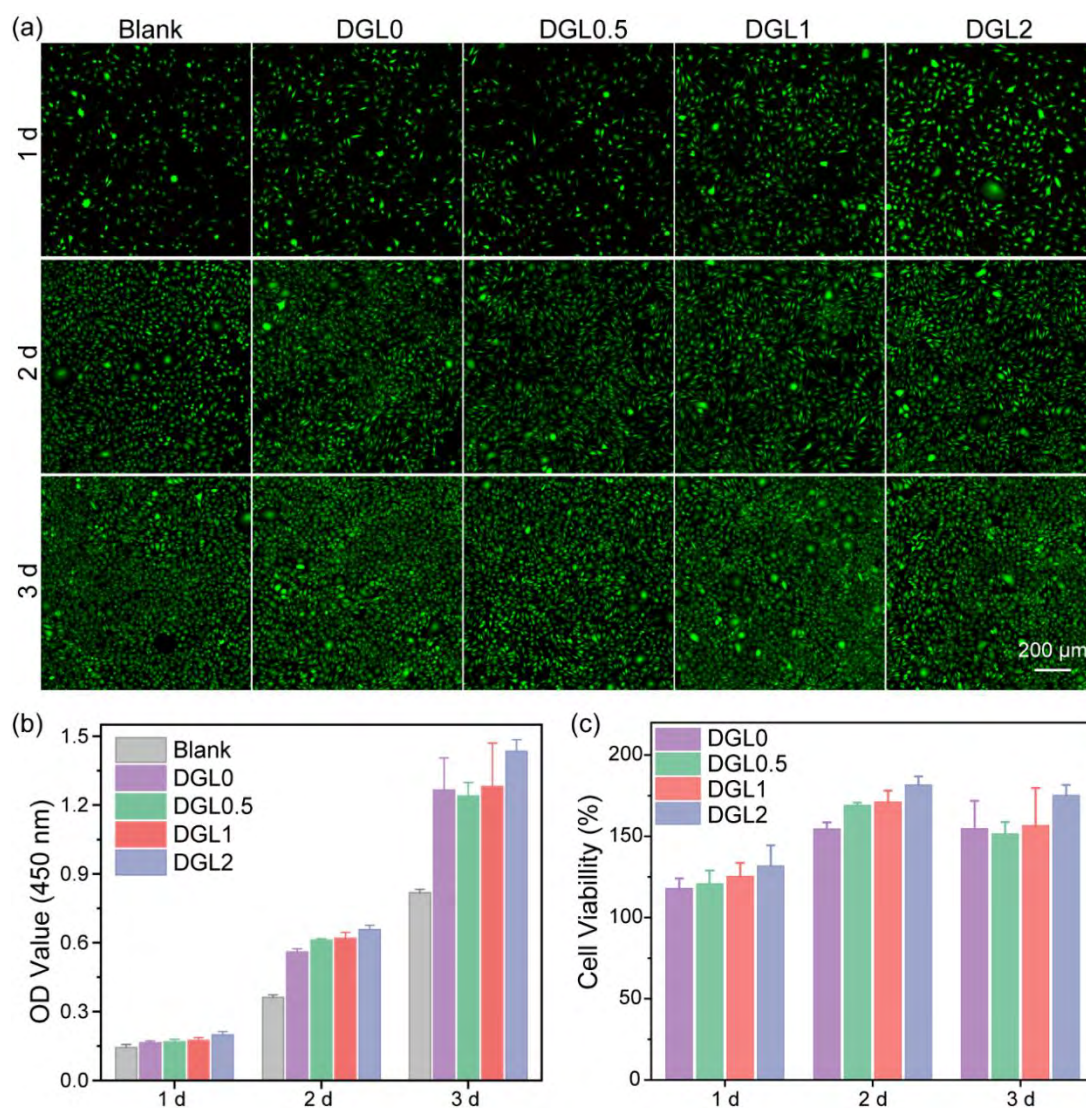
Fig. S15. *In vitro* cytocompatibility of the DGL gels: (a) Live and dead staining of the L929 cells after co-incubation with the DGL gel extracts, (b) Cell proliferation, and (c) Cell viability after co-incubation with the DGL gel extracts (n = 5).
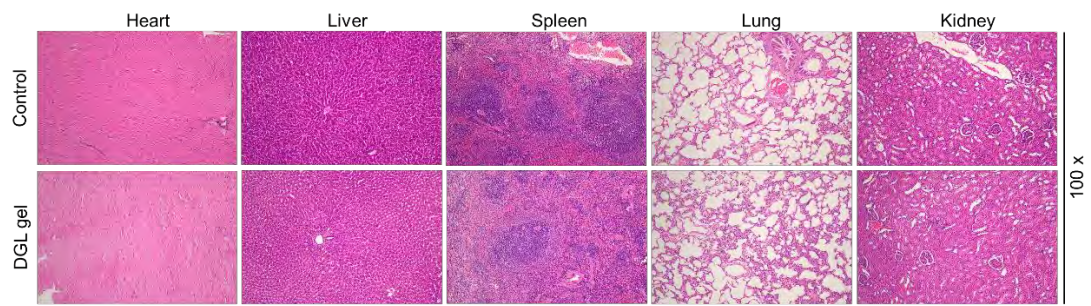
Fig. S16. H&E staining of major organs (heart, liver, spleen, lung and kidney) after subcutaneous implantation of DGL1 gel sealant in the backs of Sprague Dawley rats for 5 days.
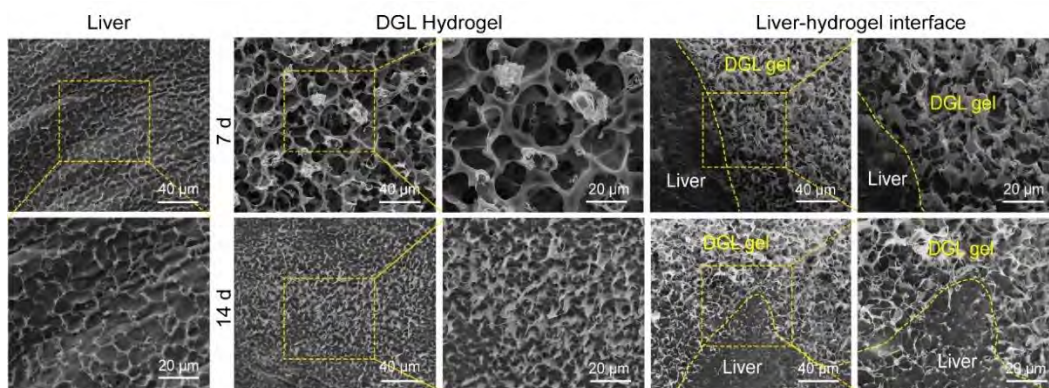
Fig. S17. Scanning electron micrographs of the residue of DGL sealants on the liver surface 7 and 14 days after surgery.
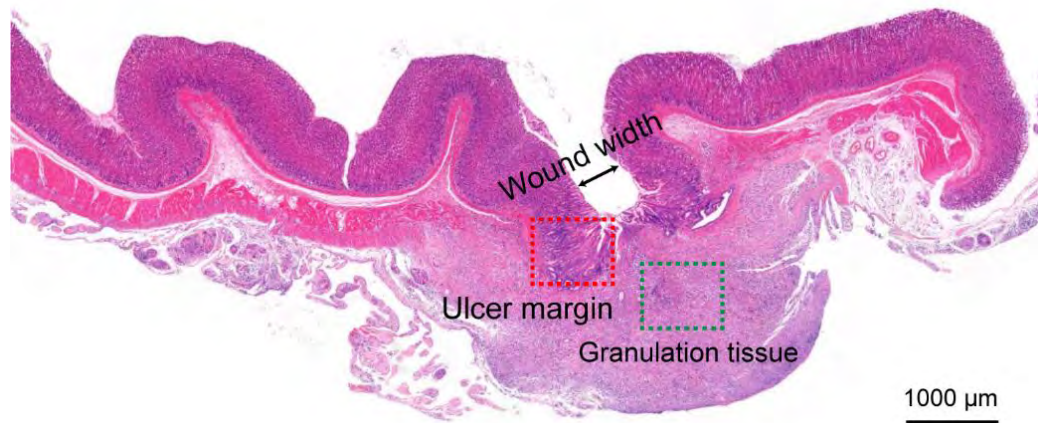
Fig. S18. H&E staining image of the gastric gap injury with the arrow distance being the width of the wound, red box demarcating the edge of the ulcer wound, and green box showing the granulation tissue.
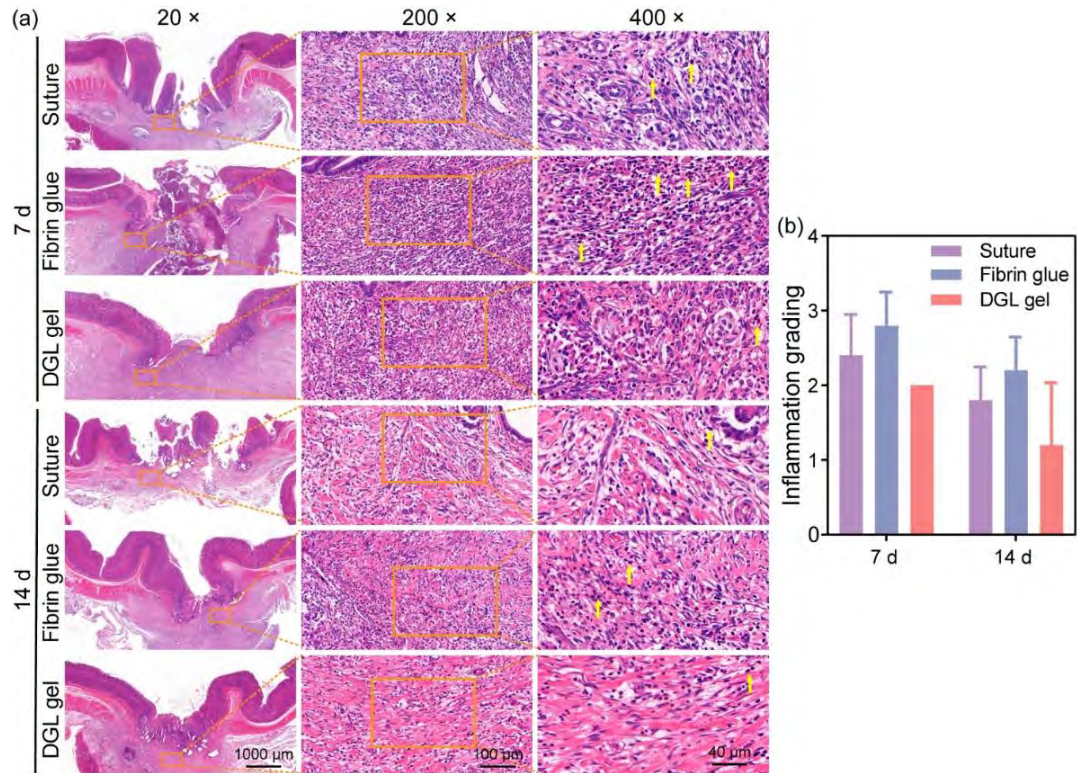
Fig. S19. Inflammation of the gastric perforation wound: (a) Representative images of granulation tissue inflammation infiltration and (b) Inflammation levels of the gastric perforation wounds treated with suture, fibrin glue, or DGL sealant on the 7th and 14th day (arrow: inflammatory cells).

Supplementary Movies:

1. Injectability of the DGL1 pregel

2. Burst pressure test of the DGL1 sealant

3. DGL sealant adhering to pigskin under twisting

4. Rat liver hemorrhage experiment of the untreated group

5. Liver hemorrhage experiment of the rat treated with the fibrin glue

6. Liver hemorrhage experiment of the rat treated with the DGL sealant

7. Large liver defect sealed by the DGL sealant

8. DGL sealant sealing the gastric perforation wound

References:

[1] Xu, M.; Li, Q.; Xie, M.; Jia, Y.; Yang, Y.; Chen, Y., Engineering air-in-water emulsion as adaptable multifunctional sealant, *Chem. Eng. J.* **2022**, 429, 132200

[2] Xu, M.; Li, Q.; Fang, Z.; Jin, M.; Zeng, Q.; Huang, G.; Jia, Y. G.; Wang, L.; Chen, Y., Conductive and Antimicrobial Macroporous Nanocomposite Hydrogels Generated from Air-in-Water Pickering Emulsions for Neural Stem Cell Differentiation and Skin Wound Healing. *Biomater. Sci.* **2020**, *8* (24), 6957-6968.